



Infrared Spectroscopic and Physical Properties of Methanol Ices—Reconciling the Conflicting Published Band Strengths of an Important Interstellar Solid

Reggie L. Hudson¹ , Perry A. Gerakines¹ , and Yukiko Y. Yamall^{1,2,3} ¹ Astrochemistry Laboratory, NASA Goddard Space Flight Center, Greenbelt, MD 20771, USA; reggie.hudson@nasa.gov² Center for Space Sciences and Technology, University of Maryland, Baltimore County, Baltimore, MD 21250, USA³ Center for Research and Exploration in Space Science and Technology, NASA Goddard Space Flight Center, Greenbelt, MD 21250, USA

Received 2023 August 6; revised 2024 April 5; accepted 2024 April 30; published 2024 July 23

Abstract

Infrared spectroscopic observations have established the presence of solid methanol (CH₃OH) in the interstellar medium and in solar system ices, but the abundance of frozen CH₃OH cannot be deduced without accurate band strengths, optical constants, and reference spectra. In this paper we identify disagreements, omissions, and gaps in the literature on infrared (IR) intensities of methanol ices, including unaddressed concerns that reach back several decades. New spectra are presented with intensity measurements aided by new data on the index of refraction and density of solid CH₃OH. The result is that the large discordant results from different laboratory groups can now be reconciled. Multiple ices have been used to determine, apparently for the first time, IR intensities of H₂O + CH₃OH mixtures of accurately known composition for use with observations of interstellar ices. Also for the first time, measurements on CH₃OH ices with different thicknesses have allowed us to report both near-IR band strengths and optical constants for two near-IR features used by planetary scientists. We have used our new IR results to determine vapor pressures of solid CH₃OH and have compared them to measurements made with a quartz-crystal microbalance. Thermal annealings of methanol ices have been carried out and phase changes in the solid state examined. Comparisons of our results to earlier work are presented where possible, and electronic versions of our new results are made available.

Unified Astronomy Thesaurus concepts: [Interstellar molecules \(849\)](#); [Astrochemistry \(75\)](#); [Laboratory astrophysics \(2004\)](#); [Chemical abundances \(224\)](#); [Ice spectroscopy \(2250\)](#)

1. Introduction

For the past decade, our group has been engaged in measuring and evaluating the infrared (IR) intensities of organic and inorganic molecules either known or suspected to exist in the solid state in extraterrestrial environments, such intensities being needed to convert IR spectroscopic observations into molecular abundances. However, the published IR intensities of methanol (CH₃OH), one of the more important molecular ices, are somewhat confusing and even contradictory, with a variety of procedures, assumptions, and IR resolutions being used by experimentalists. The result is that despite nearly 40 yr of work, one finds discordant IR intensities for CH₃OH in the refereed literature from measurements that have not received independent examination. The purpose of this paper is to reconcile such differences, examine spectral changes with temperature, and document transformations involving solid methanol. Here we report new IR spectroscopic measurements of CH₃OH ices with quantitative intensity comparisons to the extent the literature allows. Two applications also are included, the first of their type in each case.

Methanol occupies a near-unique position among extraterrestrial organic molecules in that it has been reported in the gas phase in comets (Bockelée-Morvan et al. 1991) and the interstellar medium (ISM; Ball et al. 1970) and in the solid phase in interstellar clouds (Allamandola et al. 1992) and on the Centaur object Pholus (Cruikshank et al. 1998). Methanol is one of the first three-element organics to have been detected in

the ISM, being only a year behind the first, H₂CO (Snyder et al. 1969; Ball et al. 1970). Moreover, interstellar and cometary methanol often is among the more abundant compounds in each environment.

From the vantage point of reaction chemistry, solid methanol is extremely versatile in its modes of formation and destruction. It can be produced radiolytically and photolytically from H₂O + CO and H₂O + CH₄ ices, and by low-temperature surface reactions from solid carbon monoxide, CO, one of the more common interstellar and solar system ices (e.g., Moore & Hudson 1998; Hudson & Moore 1999; Hidaka et al. 2004). Conversely, CH₃OH-ice is readily decomposed to give products such as CO, CO₂, and CH₄, plus at least one ion (HCOO[−]), one free radical (HCO), and one more-complex compound (ethylene glycol), all identified with IR methods in the solid state (Allamandola et al. 1988; Hudson & Moore 2000). Laboratory astronomers also find methanol attractive, as it is readily available, relatively inexpensive, safely handled and safely disposed of by standard laboratory methods, and it is easy to both vaporize and condense in vacuum lines.

For methanol and other astronomical ices, the spectral region of interest for identifications and quantifications is the infrared. However, converting spectroscopic observations of solid CH₃OH into molecular abundances, for either laboratory work or astronomical observations, requires spectral intensities in the form of either band strengths or optical constants that are derived from laboratory studies. Along these lines, we have published new laboratory measurements of the IR spectral intensities of about 40 molecular ices of astrochemical interest. Our group's initial work concerned five Titan nitriles (Moore et al. 2010), followed by new studies of C₂H₂ (Hudson et al. 2014a) and then C₂H₄ and C₂H₆ (Hudson et al. 2014b). Errors in the spectroscopic literature for these compounds were identified and

corrected, some having long histories. Next were our investigations of solid CH₄ and CO₂, in which we determined that nearly all solid samples of these molecules studied by laboratory astrochemists over the past ~30 yr were crystalline, and not the amorphous solids usually assumed (Gerakines & Hudson 2015a, 2015b). Investigations of almost all of the common families of organic compounds have followed (Materese et al. 2021). To date, we have reported reference spectra and IR intensities for the smallest member of most types of organic compounds except the alcohols, and so here we consider methanol (CH₃OH), the smallest member of that set.

Our most recent study of methanol was in a paper introducing a computer program for calculating optical constants (Gerakines & Hudson 2020) in which we discovered that the mid-IR optical constants $k(\tilde{\nu})$ in the literature for amorphous CH₃OH were about 50% higher than what we measured (Gerakines & Hudson 2020). Luna et al. (2018) reported a similar discrepancy earlier using a lower spectral resolution, but in neither their paper, nor in ours, was an explanation offered. At present, there are four sets of contradictory band strengths for amorphous CH₃OH in the literature. We also have found that although methanol ices have been of astrochemical interest for several decades, there still are few results in the literature on the near-IR intensities of solid CH₃OH, despite their potential use within the planetary-science community. Similarly, few measurements of IR intensities of H₂O + CH₃OH ices have been reported, despite such ice mixtures being of interest to interstellar observers from at least the 1990s (e.g., Allamandola et al. 1992) through recent work with the James Webb Space Telescope (JWST) by McClure et al. (2023).

To address the contradictions and gaps in the literature just described, here we report a fresh investigation of CH₃OH ices to determine IR reference spectra, optical constants, and band strengths. Our results have been aided by new determinations of solid methanol’s refractive index and density, quantities often hard to find in the literature. The mid- and near-IR regions used to identify solid methanol in the ISM and on solar system objects are covered, and although we are interested primarily in amorphous CH₃OH, we present new information for crystalline CH₃OH as well. The reversibility, or lack thereof, of spectral features with temperature is examined, as are both spectral changes involving crystallization and the vapor pressures of the resulting crystalline ice. We also report what appear to be the first direct measurements of near-IR band strengths for CH₃OH using a Beer’s Law approach and mid-IR band strengths for H₂O + CH₃OH mixtures prepared by a method that ensures an accurately known methanol concentration. In addition, we have applied our new IR results to measure vapor pressures of solid CH₃OH, and have confirmed the results independently with a nonspectroscopic method.

Before describing our new work, we emphasize that band strengths and optical constants of CH₃OH are as valuable to laboratory astrochemists as to astronomical observers. Studies of the photochemistry of CH₃OH-containing ices (Allamandola et al. 1988) and our own work on the radiation chemistry of CH₃OH ices (e.g., Moore & Hudson 1998) required band strengths, and usually those from either d’Hendecourt & Allamandola (1986) or Hudgins et al. (1993) were used, band strengths that we now recognize as somewhat problematic (vide infra). Subsequent IR-based laboratory explorations of chemical reactions involving CH₃OH ice have used published band strengths and optical constants, often based on a foundation of liquid-phase data for understanding ice chemistry near 10 K (e.g., Hudson and

Moore 1999; Palumbo et al. 1999; Bennett et al. 2007). In fact, it is safe to say that essentially all IR studies of CH₃OH-containing ices of the past 30 yr, in which much of the earliest work has been repeated and extended, have adopted the same band strengths in one form or another. Such published mid-IR data have even served as a foundation for extending quantitative spectral measurements into both the near- and far-IR regions (Gerakines et al. 2005; Giuliano et al. 2014). Clearly, the IR band intensities of CH₃OH are of widespread interest and value within both the laboratory astrochemical and observational astronomy communities.

2. Background to Measurements

Infrared spectral intensities of CH₃OH ices are the main topic of this paper, so we begin by describing their measurement. Readers either familiar with or uninterested in such background material might wish to skip this Section.

Within the laboratory astrochemistry community, the most common ways to express IR intensities of ices are band strengths (A'), absorption coefficients (α'), and the complex refractive index, $n(\tilde{\nu}) - ik(\tilde{\nu})$, with optical constants $n(\tilde{\nu})$ and $k(\tilde{\nu})$. Equation (1) is used to measure A' for an IR band, and Equation (2) is used to measure α' for an IR absorbance peak, with h in each case representing ice thickness or IR pathlength, which are the same in our work.

$$\int_{\text{band}} (\text{Absorbance}) d\tilde{\nu} = \left(\frac{\rho_N A'}{2.303} \right) h \quad (1)$$

$$\text{Absorbance} = \left(\frac{\alpha'}{2.303} \right) h \quad (2)$$

To use Equation (1) to find a band strength A' , one also needs the ice sample’s number density, $\rho_N = \rho (N_A/M)$, where ρ is mass density, N_A is Avogadro’s constant (i.e., 6.022×10^{23} molecules mole⁻¹), and M is the molar mass of the ice (g mole⁻¹), giving ρ_N , the ice’s number density, in units of molecules cm⁻³.

These two equations are, of course, just forms of Beer’s Law (or the Beer–Lambert Law). To use the first equation, one prepares a set of ice samples of different thicknesses, records their spectra, and integrates the IR bands of interest. The integrals then are graphed as a function of h , the resulting linear trend having a slope ($\rho_N A'/2.303$) from which band strength A' is found if number density ρ_N is known. A similar graph of absorbance of an IR peak of an ice as a function of h yields a linear trend with, according to Equation (2), a slope of ($\alpha'/2.303$) from which α' is calculated. The 2.303 \approx ln(10) term is needed in Equations (1) and (2) to convert the base-10 scale of most commercial spectrometers to a base-e scale.

A requirement for using Equations (1) and (2) as just described is that the ice sample’s thickness h is needed. In our work, and in much of the relevant literature, values of h are determined with interferometry. Specifically, as a sample is condensed from the vapor or gas phase onto a cold substrate, a laser of wavelength λ is used to generate a number (N_{fr}) of interference fringes from the ice-substrate interface, the laser’s beam being at an angle (θ) with respect to a line drawn perpendicular to the plane of the sample. Equation (3) is the relevant relation for calculating h , where n is the sample’s refractive index at λ .

$$h = \frac{N_{\text{fr}} \lambda}{2\sqrt{n^2 - \sin^2 \theta}} \quad (3)$$

Table 1
Selected Refereed Publications of Amorphous CH₃OH IR Band Strengths^a

	d'Hendecourt & Allamandola (1986)	Hudgins et al. (1993)	Palumbo et al. (1999)	Bouilloud et al. (2015)	Luna et al. (2018)
n measured ?	unknown	no	unknown	no	yes
n used	unknown	1.33 ^b	unknown	1.33 ^b	1.257
ρ measured ?	no	no	unknown	no	yes
ρ used	1.00 ^b	1.00 ^b	unknown	1.01 ^b	0.636
Integration limits	unknown	unknown	unknown	unknown	specified
IR spectral resolution/cm ⁻¹	2	1 ^c	2	1	2
Beer's Law plots prepared ?	unknown	unknown	unknown	yes	yes
Spectra available in electronic files ?	no	yes	no	no	no

Notes.

^a Ice temperatures are 10–25 K.

^b Value assumed, not measured, in the paper cited.

^c Spectra recorded at a resolution of 0.9 cm⁻¹ and published at intervals of both 0.9 and 1 cm⁻¹, slightly degrading the resolution to about 2 cm⁻¹.

Table 2
Selected Refereed Publications of Amorphous CH₃OH IR Optical Constants^a

	Hudgins et al. (1993)	Rocha & Pilling (2014)	Luna et al. (2018)	Gerakines & Hudson (2020)
n measured ?	no	no	yes	yes
n used	1.33 ^b	unknown ^c	1.257	1.296
Multiple ices used ? ^d	unknown	unknown	yes	yes
IR spectral resolution/cm ⁻¹	1 ^c	unknown	2	1
IR spectra shown ?	yes	no	yes	yes
Optical constants available in electronic files ?	yes	yes	no	yes
Software released ?	no	yes	no	yes

Notes.

^a Ice temperatures are 10–20 K.

^b Value assumed, not measured, in the paper cited.

^c The value in Table 1 of Rocha & Pilling (2014) disagrees with the work cited (Hudgins et al. 1993). Also, ice thicknesses were determined with band strengths taken from the literature, but neither citations nor band-strength values nor their method of measurement were given.

^d Refers to ices with different thicknesses.

^e Spectrum recorded at a resolution of 0.9 cm⁻¹ and published at intervals of both 0.9 and 1 cm⁻¹, slightly degrading the resolution to about 2 cm⁻¹.

For the new results in this paper and for what follows in this Section, $\theta \approx 0^\circ$, so Equation (3) reduces to:

$$h = \frac{N_{fr} \lambda}{2n}. \quad (4)$$

The previous equations show that both n and ρ are needed to determine an ice's A' and α' values using graphs based on Equations (1) and (2). Here we report not only new results for A' and α' for CH₃OH ices, but also new measurements of n and ρ on which band strengths and absorption coefficients are based.

The main use of solid-phase IR spectral intensities by astronomers is to convert observational spectra of icy solids in extraterrestrial environments into molecular column densities. The column density N , usually in molecules cm⁻², of an extraterrestrial ice component can be found from the ice's IR spectrum by integrating an absorbance feature over a wavenumber ($\tilde{\nu}$ in cm⁻¹) range, converting absorbance to optical depth (τ) with $\tau = \text{absorbance} \times \ln(10)$, and then dividing the resulting integral by the appropriate band strength A' (in cm molecule⁻¹) as in Equation (5). See McClure et al. (2023) for recent JWST examples.

$$N = \frac{\int_{\text{band}} (\tau) d\tilde{\nu}}{A'} \quad (5)$$

To summarize, molecular abundances in either laboratory or extraterrestrial ices can be found from IR spectra using Equation (5) if IR band strengths (A') are known, but these depend on knowing the appropriate n - and ρ -values.

Returning to Equation (2), absorption coefficients α' are not used as widely as band strengths, but they are a rapid, convenient, and quantitative way to compare intensities of spectra from different laboratories. See Quirico & Schmitt (1997) for an extensive set of near-IR spectra with intensities expressed as absorption coefficients, with an eye toward applications to trans-Neptunian objects (TNOs).

A different way to quantify IR spectral intensities of ices is with the complex refractive index, $n(\tilde{\nu}) - ik(\tilde{\nu})$, with optical constants $n(\tilde{\nu})$ and $k(\tilde{\nu})$. Although the computation of optical constants is more difficult than determining α' or A' , $n(\tilde{\nu})$ and $k(\tilde{\nu})$ can be used to calculate a spectrum for different ice thicknesses over a range of wavenumbers (wavelengths) and to mathematically model IR spectra of extraterrestrial surfaces and atmospheric ices.

3. Some Earlier Laboratory Work on Methanol

Tables 1 and 2 list some of the key refereed papers on IR intensities of solid CH₃OH along with some important points related to them. Even a cursory glance at these two tables reveals the challenge in making meaningful, quantitative comparisons of IR intensities. Factors such as ice density and

refractive index, the number of ices examined, spectral resolution, and integration limits, not to mention sample temperature, baseline choices, and, if used, curve fitting routines, can influence published IR band strengths. Put another way, it is easy to list band strengths from different laboratories, but critical comparisons of quantitative results need to consider the influences just mentioned to be meaningful; otherwise, agreements or disagreements between laboratories can be considered as little more than fortuitous.

To our knowledge, the earliest relevant work on solid-methanol IR band strengths is that of d’Hendecourt & Allamandola (1986), who published IR spectra of amorphous CH_3OH near 10 K at a resolution of 2 cm^{-1} . A density of $\rho = 1\text{ g cm}^{-3}$ was assumed, but the ice’s refractive index (n), needed to determine a thickness (and IR pathlength), was not stated. Infrared band areas were calculated with a numerical approximation related to bandwidth and peak height, after conversion to an optical-depth scale, but the approximation used by the authors is incorrect. Specifically, the text refers to IR band shapes as Lorentzian, but the area under a Lorentzian curve is about 57% larger (a factor of $\pi/2$) than given by the authors’ equation (see G nzler & Gremlich 2002). If the band shapes of d’Hendecourt & Allamandola (1986) were indeed Lorentzian, then an error of about 57% has existed in the astrochemical literature for over 30 yr. Also uncertain are (i) the number of ices examined, (ii) the thicknesses of the methanol ices studied, and (iii) the baselines used for integrating some of the weaker IR bands that overlapped with stronger features (e.g., $3000\text{--}2800\text{ cm}^{-1}$). For these reasons, we recognize the early work of d’Hendecourt & Allamandola (1986) as a pioneering study that has been superseded by the other measurements cited in Table 1. It is not used in the rest of this paper.

Table 1 shows that the work just described was first followed by a publication from Hudgins et al. (1993) on IR band strengths, a work that has assumed a near-classic status for those in the field. Faced with a lack of supporting data, the authors used liquid methanol’s refractive index of $n = 1.33$ ($\lambda = 632.8\text{ nm}$) and an assumed density of $\rho = 1\text{ g cm}^{-3}$ for all of their amorphous and crystalline ices from $10\text{--}120\text{ K}$. Band strengths were calculated from spectra with a resolution of 0.9 cm^{-1} , but the spectra’s publication at wavenumber intervals of 0.9 and 1 cm^{-1} degrades the resolution to about 2 cm^{-1} . The authors’ IR spectra and numerical results were presented in extensive printed tables and later posted in digital form on the authors’ website.

Continuing to the right in Table 1, Palumbo et al. (1999) reported IR band strengths for amorphous CH_3OH , apparently at 10 K. Interference fringes were said to have been used to calculate ice thickness, but the refractive index assumed or measured was not given. Also unstated was the ice’s density, which was needed to calculate A' . Integration limits were not provided, and the spectral resolution (2 cm^{-1}) was less than that of Hudgins et al. (1993). Finally, as with the two earlier papers in Table 1, it is not known if more than one ice was examined. The paper of Palumbo et al. (1999) is not used in the rest of this paper due to these uncertainties and concerns.

Table 1 shows that in a subsequent investigation of amorphous solid CH_3OH , Bouilloud et al. (2015) returned to a resolution of 1 cm^{-1} for IR measurements, but for their analysis of IR spectra for amorphous solid methanol, the authors adopted a density of *crystalline* methanol and a *liquid*-phase value for the refractive index. Even after allowing for the

slightly different densities used, the band strengths of Hudgins et al. (1993) were still significantly larger than those of Bouilloud et al. (2015). For example, for the two largest IR bands, the Hudgins et al. (1993) band strength was 57% larger near 3200 cm^{-1} and 67% larger near 1020 cm^{-1} , a striking contradiction from 22 yr earlier that still resides in the literature. We mention in passing that variations in refractive indices in Table 1 and our own work (vide infra) are much smaller than density differences, and so have relatively little influence on reported band strengths.

Of the published work on methanol’s IR intensities in Table 1, the most recent is that of Luna et al. (2018), who measured and stated the refractive indices and densities of solid CH_3OH . For the first time, integration limits were provided to aid in reproducing the results, although the spectral resolution adopted by the authors was less than that of 25 yr earlier. The spectra published resemble those in the literature, but later in this paper we raise questions about the authors’ refractive indices and densities, and therefore about the resulting band strengths for solid methanol.

The literature on methanol-ice’s IR optical constants is even sparser than that for IR band strengths, with selected refereed publications being summarized in Table 2. Again, Hudgins et al. (1993) assumed n and density values for their ices in the absence of measured values. Those authors published IR spectra and optical constants $n(\tilde{\nu})$ and $k(\tilde{\nu})$ both in extensive tables and figures in their paper. The most serious concern, which we address later, is that only one methanol ice was used to measure optical constants.

The paper of Rocha & Pilling (2014) on optical constants of solid CH_3OH was the first to release the software needed for calculating $n(\tilde{\nu})$ and $k(\tilde{\nu})$. However, that study is severely compromised by the omission of the underlying band strengths, refractive indices, densities, and associated citations used. Neither the number nor the positions of IR bands used for determining ice thickness were stated, nor was the number of ices examined. No ranges were supplied for the integrations used to determine ice thickness, no spectral resolution was given, and no IR spectra were shown. We also note that the units in the authors’ Equation (1) do not cancel properly and that the numerical conversion is off by a factor of 10. Also, the authors’ Equation (2) suggests that absorbance is defined with base-10 (common, Briggsian) logarithms, which contradicts the base-e (natural, Napierian) logarithms of Equation (3). It is not clear if these points influenced the final published results, but because of them, quantitative comparisons to those same results cannot be confidently and usefully made. The paper of Rocha & Pilling (2014) is listed in Table 2, but we do not use it in what follows.

The work of Luna et al. (2018), as already mentioned, included measurements of n for solid CH_3OH . The results were used by the authors to calculate optical constants $n(\tilde{\nu})$ and $k(\tilde{\nu})$, although again with a spectral resolution (2 cm^{-1}) less than that from 25 yr earlier (i.e., Hudgins et al. 1993). The optical constants of Hudgins et al. (1993), which are available electronically in digital form, were used for comparison, but the authors’ own $n(\tilde{\nu})$ - and $k(\tilde{\nu})$ -values were not presented in the same way, only as figures, hindering comparisons, verification, and adoption. Eight sets of $n(\tilde{\nu})$ - and $k(\tilde{\nu})$ -values were shown in one figure as overlapping traces in a single panel, making digitization difficult. No software was released, again hindering comparisons and independent verifications.

The final column of Table 2 refers to a small part of a publication describing our open-source program for calculating optical constants of ices (Gerakines & Hudson 2020). It was while working on that paper that we first noticed a disagreement and gaps in the literature on IR intensities of solid CH₃OH. The present paper greatly expands on that work, proposing a resolution of the disagreement and making suggestions on how to avoid such problems in the future.

To conclude this Section, the relevant literature on IR intensities of CH₃OH ices contains unstated and assumed physical constants, a room-temperature liquid-phase refractive index for a 10 K amorphous ice, a crystalline solid's density for an amorphous sample, a lack of tabulated optical constants, and a lack of computer codes by which results can be independently verified and confidently used. There is also the unconventional practice of using a single sample to, in effect, determine a calibration curve. All of this clearly constitutes an unsatisfactory situation for one of the more common organic molecules in interstellar and planetary environments. Not surprisingly, such problems lead to differences in CH₃OH band strengths used by astronomical observers and, in turn, molecular abundances based on observations. For example, the A' near 1027 cm⁻¹ for solid CH₃OH cited in a recent JWST publication on interstellar ices (McClure et al. 2023) is from the oldest paper (d'Hendecourt & Allamandola 1986) in Table 1, a paper with the lowest resolution listed and that has long since been superseded by other work. The substantial differences between the methanol band strengths of Hudgins et al. (1993) and Bouilloud et al. (2015) have already been mentioned, two studies that used the same IR spectral resolution but with neither work having a measured amorphous-CH₃OH density on which to base a band strength. Just as troubling are significant differences in the optical constants calculated by Hudgins et al. (1993) and Luna et al. (2018), specifically the $k(\bar{\nu})$ -values of Hudgins being about 50% higher than those of Luna et al. (2018).

What is required is a new first-principles IR study of CH₃OH infrared band strengths with values of density and refractive index measured for methanol ices, with both optical constants and computer code available electronically, and with a spectral resolution that is at the limiting value for the compound and near that of JWST. The present paper is such an investigation. Along with these studies of IR intensities, we also examine the thermal annealing on methanol ices and document phase changes in CH₃OH ices.

4. Laboratory Methods

Our methods and equipment have been described in publications on band intensities for, as examples, CO, CO₂, N₂O, HCN, NH₃, and hydrocarbons (e.g., Hudson 2017; Hudson et al. 2022a; Gerakines et al. 2022). Briefly, high-purity methanol was purchased from Sigma Aldrich and used as received except for standard degassing. (A few experiments were carried out with triply distilled, degassed H₂O with a resistivity greater than 10⁷ ohm cm.) Methanol ices were made by condensation of room-temperature CH₃OH vapor onto a CsI or KBr substrate held at the temperature of interest inside a high-vacuum chamber (~10⁻⁸ Torr at room temperature). The cryostat's minimum temperature during the course of our work varied from about 9–11 K, which for simplicity we refer to as just 10 K. Laser interferometry was used to measure the thickness of each methanol sample studied (Heavens 1955, Hollenberg & Dows 1961; Groner et al. 1973; Heavens 2011).

The CH₃OH deposition rate was equivalent to an increase in ice thickness of about 1 μm hr⁻¹ in most cases, although a few ices were made at slightly higher rates, with no spectral differences found.

Five H₂O + CH₃OH ice mixtures with a molecular (molar) ratio of 10:1 were prepared as described in Yarnall & Hudson (2022b), with ice thickness being between about 0.25 and 1.00 μm (one to four interference fringes).

Infrared spectra were recorded in transmission using a Thermo iS50 FTIR spectrometer (DTGS detector) with the IR beam perpendicular to the sample (Moore et al. 2010), typically as 200-scan accumulations from 5000 to 400 cm⁻¹ at 1 cm⁻¹ resolution. Band areas at 1 cm⁻¹ resolution were a few percent larger than those at 2 cm⁻¹ resolution, but essentially the same as at 0.5 cm⁻¹ resolution. In short, our 1 cm⁻¹ spectra were not resolution limited. They also were comparable to the ~1 cm⁻¹ resolution of JWST's NIRSpec instrument in the 3700–1900 cm⁻¹ region (McClure et al. 2023).

Densities (ρ) of solid CH₃OH were measured by microgravimetry (Lu & Lewis 1972), and two-laser interferometry ($\lambda = 670$ nm) was used to determine refractive indices (n_{670}) as before (Tempelmeyer & Mills 1968; Hudson et al. 2017), the ρ and n_{670} measurements being made simultaneously in a UHV chamber (~10⁻¹⁰ Torr). See Hudson et al. (2017) for examples of interference patterns and microbalance output.

A quartz-crystal microbalance (QCM) in this same UHV chamber was used to measure vapor pressures as in our recent paper on benzene (Hudson et al. 2022b), but pressures also were determined by an infrared method proposed by Khanna et al. (1990). For the QCM work, an ice was grown on the gold-coated surface of our quartz-crystal microbalance and then warmed while the temperature and the microbalance's frequency were recorded. As the ice sublimed, the microbalance's frequency increased, and by comparison to the balance's frequency on warming with no sample present, the methanol mass loss was calculated and from it a vapor pressure was found. See Hudson et al. (2022b) for the relevant equations. See Khanna et al. (1990) for details of the IR method used for vapor-pressure measurements.

Uncertainties in our measurements of IR intensities are mainly from uncertainties in ice thicknesses measured by interferometry. As in our recent CO paper (Gerakines et al. 2023), the uncertainty in our fringe counts is about a tenth of a fringe, which corresponds to a methanol ice thickness of about 0.026 μm = 2.6 × 10⁻⁶ cm. Using this uncertainty in h in a least-square routine gave uncertainties in slopes of our Beer's Law plots of about 5%, which corresponds to the uncertainty in our mid-IR band strengths, A' . The value for near-IR A' -values is somewhat larger, 8%–10%, due to the weakness of each band and the need for channel-fringe removal. Our recent paper on allene's IR intensities gives additional information on the methods we used (Hudson & Yarnall 2022).

Our paper on benzene's vapor pressures contains an analysis of measurements with our microbalance method (Hudson et al. 2022b). There we estimated an uncertainty in vapor pressures of about 1% over the temperatures and pressures studied, which are similar to those used here. Our enthalpy of sublimation's uncertainty there was < 0.5 kJ mol⁻¹, but here we suggest ±0.5 kJ mol⁻¹ due to the somewhat smaller temperature range (fewer data points) for methanol sublimation.

5. Results

Solid methanol under vacuum or low-pressure conditions can exist in an amorphous form and in two crystalline phases designated α and β for the low- and high-temperature forms, respectively. A reversible conversion between the α and β crystalline phases occurs near 157 K (Carlson & Westrum 1971) and has been studied for nearly a century to elucidate structural and thermodynamic changes (e.g., Parks 1925; Tauer & Lipscomb 1952; Dempster & Zerbi 1971; Torrie et al. 2002). Lin et al. (2016) published a particularly thorough structural study, which can be consulted for most of the relevant literature.

Infrared spectroscopic work by, for example, Falk & Whalley (1961) and Fischer & Fuhrich (1983) showed that methanol vapor can be condensed below ~ 100 K to make an amorphous solid that undergoes crystallization to give α -CH₃OH on warming above ~ 100 K. Our own measurements, with few exceptions, were between 10 and 135 K, and so our main interests were the amorphous and α -crystalline forms of solid methanol. Under our experimental conditions and timescales, only the amorphous form and the lower-temperature (α) crystalline phase of CH₃OH were stable, as our methanol ices rapidly sublimed before the α -to- β transition temperature was reached. However, in Section 5.5 we describe how we were able to prepare β -crystalline methanol, which quickly changed into the α polymorph.

Here we first present some nonspectroscopic results, followed by measurements of IR intensities. Next come observations related to phase changes in methanol ices. We then describe two applications of our work, one concerning band strengths of H₂O + CH₃OH ices and the other a comparison of two methods for measuring vapor pressures, one of them using our new IR intensities.

5.1. Refractive Indices and Ice Densities

Conversions of the peak heights and band areas of our IR spectra to absorption coefficients, band strengths, and optical constants required refractive indices (n_{670}) and densities (ρ) of solid CH₃OH as described in Section 2. Measurements of n_{670} and ρ made in triplicate (or more) near 15 and 120 K for amorphous and crystalline methanol, respectively, were reported in previous publications (Hudson et al. 2020; Yarnall & Hudson 2022a). For the present work, we also made triplicate measurements at 50 and 80 K for amorphous CH₃OH and at 130 K for the crystalline solid. Table 3 summarizes our results, with the temperatures covering values relevant from the ISM to the Galilean satellites. The n and ρ results of Luna et al. (2018) are slightly lower than those we obtained, as shown in Figure 1. Also in Figure 1 is a density measurement at 122 K from a diffraction study of Kirchner et al. (2008). Our densities at 120 and 130 K bracket that value, giving our results support from an independent set of measurements with a different technique (Kirchner et al. 2008). The slight decrease in the crystalline ice's density with increasing temperature mirrors that in the diffraction work of Torrie et al. (1988) and Torrie et al. (2002). We return to densities and refractive indices in Section 6.

5.2. Mid-infrared Spectra and Spectral Intensities for Solid CH₃OH

Mid-infrared spectra of CH₃OH at approximately the lower four temperatures of Table 3 are shown in Figure 2. Qualitatively,

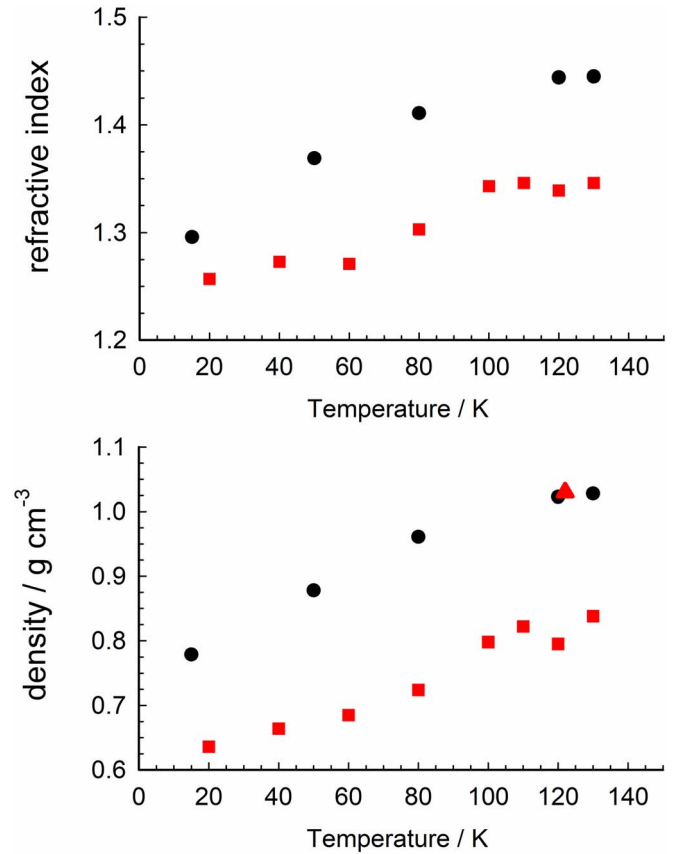


Figure 1. Refractive indices and densities of methanol ices. Black circles are from this work, red squares are from Luna et al. (2018). In the lower panel, the red triangle is for $\rho = 1.03 \text{ g cm}^{-3}$ at 122 K from a diffraction study of crystalline methanol (Kirchner et al. 2008). Our refractive indices are for $\lambda = 670 \text{ nm}$, those of Luna et al. (2018) are for $\lambda = 633 \text{ nm}$. Each ice in each study was condensed at the temperature indicated along the horizontal axis.

Table 3
Refractive Indices and Densities of Methanol Ices^{a,b}

T/K	n_{670}	$\rho/\text{g cm}^{-3}$
15	1.296	0.779
50	1.369	0.878
80	1.411	0.961
120	1.444	1.023
130	1.429	1.013

Notes.

^a Ices were made at the temperatures listed in the first column. Ices made below 120 K were amorphous, those made at 120 and 130 K were crystalline. Values of n and ρ are averages of at least three measurements. Uncertainties are about ± 0.005 and $\pm 0.005 \text{ g cm}^{-3}$ for n_{670} and ρ , respectively.

^b The values at 15 and 120 K are taken from Hudson et al. (2020) and Yarnall & Hudson (2022a), respectively.

the spectra resemble those in the papers cited in Tables 1 and 2. To measure IR band strengths, we prepared methanol ices with thicknesses from about 0.2–2 μm , recorded their spectra, and measured peak heights and band areas at 10, 50, 80, and 120 K. The results were used to calculate absorption coefficients (α' in cm^{-1}) and band strengths (A' in cm molecule^{-1}) from the appropriate Beer's Law plots, as described earlier. See Equations (1) and (2) above and the related discussion. Examples of Beer's Law plots for amorphous CH₃OH at 10 K are given in

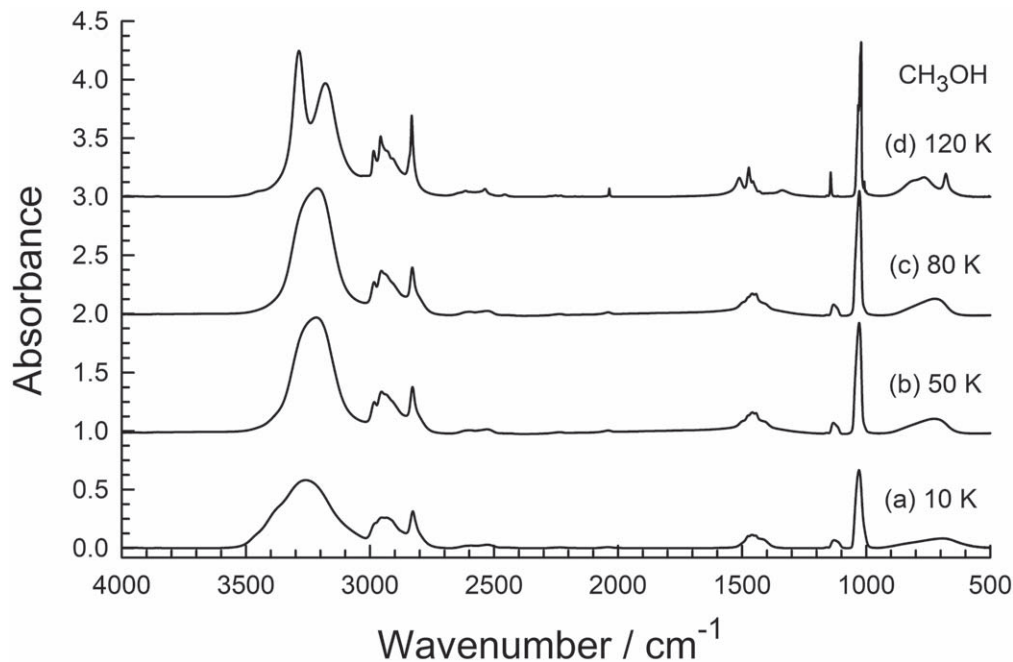


Figure 2. Infrared spectra of four CH_3OH ices, each condensed at the temperature shown and each having a thickness of about $1 \mu\text{m}$. Spectra are offset for clarity.

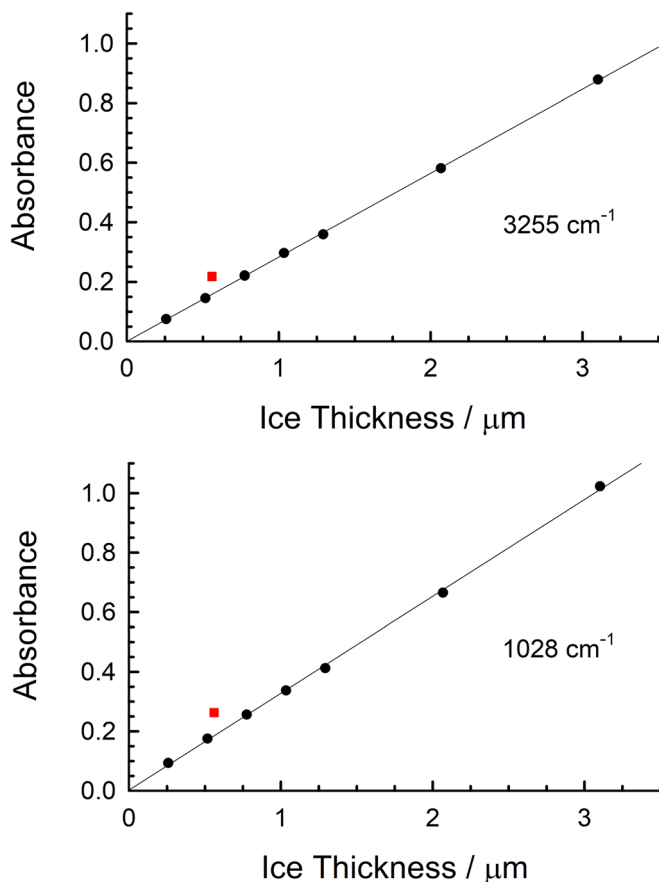


Figure 3. Comparison of results for amorphous CH_3OH at 10 K and a resolution of 1 cm^{-1} . Red squares: Hudgins et al. (1993). Black circles: this work.

Figure 3, with a point added in each graph from the work of Hudgins et al. (1993). Tables 4–7 give the values of α' and A' we measured.

We also calculated solid methanol’s optical constants $n(\tilde{\nu})$ and $k(\tilde{\nu})$ at 10, 50, 80, and 120 K using the open-source computer code of Gerakines & Hudson (2020). Figure 4 shows the results for amorphous CH_3OH at 50 K. We emphasize that our optical constants are averages of values found from the IR spectra of four or more ices, as opposed to being calculated from just a single spectrum. Links to electronic versions of our optical constants, and the software used to calculate them, are available.⁴

5.3. Near-infrared Spectra and Spectral Intensities for Solid CH_3OH

Of special interest in our work were two near-IR features between about 5000 and 4000 cm^{-1} that have been used in the study of solid CH_3OH on TNOs (Cruikshank et al. 1998). See Figure 5 for spectra in this region of amorphous and crystalline CH_3OH at the temperatures indicated, with wavelengths given for the two bands of interest. The weakness of all near-IR absorbances in this region made band-strength measurements harder than for the mid-IR features, and so ices as thick as $\sim 8 \mu\text{m}$ were examined. However, the spectra of all such ices showed pronounced channel fringes, hindering baseline determinations and intensity measurements until a simple trigonometric routine was used to remove such fringes. Although some small residual baseline uncertainties were present from 5000 – 4000 cm^{-1} , we avoided their influence by focusing on the narrower 4600 – 4200 cm^{-1} region and the two distinct IR peaks near 4398 cm^{-1} ($2.274 \mu\text{m}$) and 4273 cm^{-1} ($2.340 \mu\text{m}$) in Figure 5, those features being the most likely to lead to CH_3OH detections on TNOs. See Brunetto et al. (2005) for more on these two near-IR bands and their use.

As with our mid-IR study, we prepared CH_3OH ices with different thicknesses and recorded their spectra, focusing on results at 10 and 120 K. The 4600 – 4200 cm^{-1} region then was integrated for each ice’s spectrum at each temperature. Curve

⁴ <https://science.gsfc.nasa.gov/691/cosmicice/constants.html>

Table 4
Intensities of Selected IR Absorptions of Amorphous CH₃OH at 10 K^a

Approximate Description ^b	Peak Position/cm ⁻¹	α' /cm ⁻¹	Integration Range/cm ⁻¹	$A'/10^{-18}$ cm molecule ⁻¹
OH stretch	3259	6500
CH ₃ asymmetric stretch	2952	2900	3650–2685 ^c	152
CH ₃ symmetric stretch	2828	3470
Combination (1459, 1129)	2527	332	2685–2338	2.91
Overtone of CH ₃ rock	2233	65.3	2318–2100	0.294
Overtone of C–O stretch	2040	86.5	2100–1968	0.315
OH in-plane bend	1459	1250	1656–1310	7.69
CH ₃ rock	1129	752	1180–1070	1.91
C–O stretch	1028	7500	1070–967	16.2
OH out-of-plane bend	693	858	967–505	12.4

Notes.

^a Values of α' and A' are rounded to three significant figures. See the text for uncertainties.

^b Approximate descriptions are from Falk & Whalley (1961).

^c Note that this range covers the first three bands of the leftmost column.

Table 5Intensities of Selected IR Absorptions of Amorphous CH₃OH at 50 K^a

Peak Position/cm ⁻¹	α' /cm ⁻¹	Integration Range/cm ⁻¹	$A'/10^{-18}$ cm molecule ⁻¹
3220	11400
2983	3280	3641–2693 ^b	183
2954	4270
2828	4740
2529	425	2693–2346	3.03
2237	92.2	2299–2199	0.266
2041	152	2091–2000	0.326
1460	1940	1760–1184	15.3
1132	1080	1174–1092	1.95
1028	10800	1092–953	18.0
724	1410	953–560	14.1

Notes.

^a Values of α' and A' are rounded to three significant figures. See the text for uncertainties. Vibrational assignments and descriptions are in Table 4.

^b Note that this range covers the first four bands of the leftmost column.

Table 6Intensities of Selected IR Absorptions of Amorphous CH₃OH at 80 K^a

Peak position/cm ⁻¹	α' /cm ⁻¹	Integration Range/cm ⁻¹	$A'/10^{-18}$ cm molecule ⁻¹
3212	13000
2984	3490	3641–2684 ^b	177
2954	4610
2830	5260
2528	480	2684–2383	3.34
2236	96.1	2299–2199	0.241
2040	188	2098–2000	0.336
1458	2130	1760–1192	16.5
1132	1110	1192–1097	1.71
1026	12600	1097–953	17.5
721	1620	953–560	1.31

Notes.

^a Values of α' and A' are rounded to three significant figures. See the text for uncertainties. Vibrational assignments and descriptions are in Table 4.

^b Note that this range covers the first four bands of the leftmost column.

Table 7Intensities of Selected IR Absorptions of Crystalline CH₃OH at 120 K^a

Peak Position / cm ⁻¹	α' /cm ⁻¹	Integration Range/cm ⁻¹	$A'/10^{-18}$ cm molecule ⁻¹
3287	15,600
3178	11,100
2985	4390	3545–2700 ^b	174
2957	6400
2832	8410
2537	691	2700–2424	3.57
2251	122	2290–2203	0.235
2035	956	2076–2010	0.302
1511	2050
1473	3330	1750–1170	12.7
1337	627
1143	2960	1170–1120	0.826
1020	14,900	1070–948	13.7
766	2080	948–583	16.4
679	2710

Notes.

^a Values of α' and A' are rounded to three significant figures. See the text for uncertainties. Vibrational assignments and descriptions are in Table 4.

^b Note that this range covers the first five bands of the leftmost column.

fitting (Voigt functions) with five ices revealed that the area of the feature at ~ 4398 cm⁻¹ in Figure 5 was about 5.3 times greater than the area of the ~ 4273 cm⁻¹ band. The usual Beer's Law plot of area as a function of ice thickness was constructed to give the integrated intensity over the entire 4600–4200 cm⁻¹ region, from which the 5.3:1 ratio allowed us to calculate the band strength for each of the two absorbances. Results are in Table 8 for the amorphous and crystalline CH₃OH at 10 and 120K, respectively. Near-IR optical constants were calculated and are shown in Figure 5.

5.4. Temperature Changes and Spectra of Solid CH₃OH

Infrared spectra of solid methanol either warmed (Hudgins et al. 1993) or cooled (Drobyshv et al. 2019) have been published, but spectra showing the results of various annealings are harder to find. Therefore, in Figures 6–8 we present IR

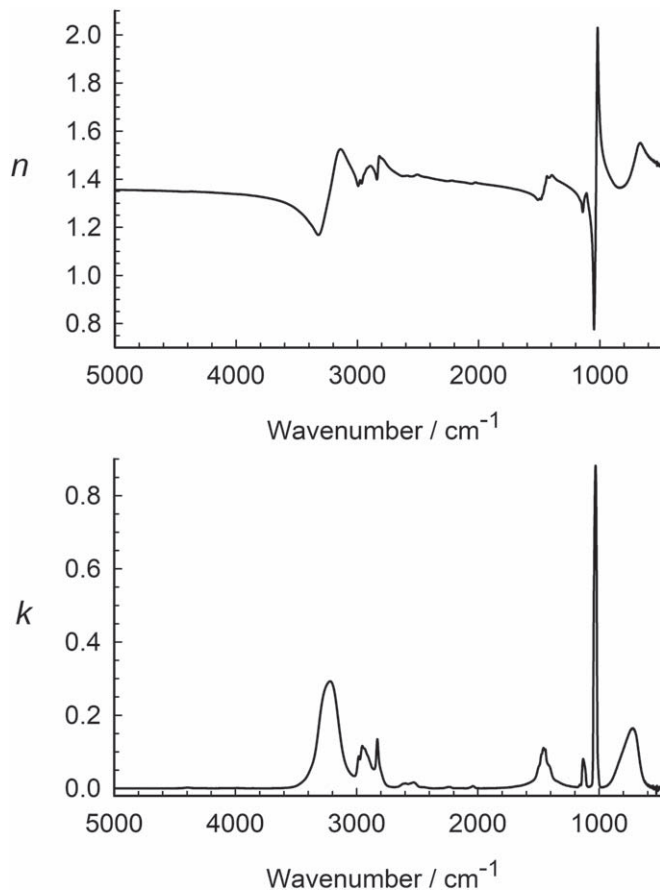


Figure 4. Optical constants of amorphous methanol at 50 K.

spectra for CH_3OH ices that have been annealed, meaning warmed and then cooled.

Figure 6 shows IR spectra for an amorphous CH_3OH sample made at 10 K and then warmed to 90 K. Thermally induced changes are seen on going from (a) to (b), mainly consisting of a slight narrowing of IR bands, an increase in absorbance near 3300 cm^{-1} relative to that near 1000 cm^{-1} , and slightly improved resolution of the features near $3000\text{--}2900\text{ cm}^{-1}$. That these changes were irreversible is seen by comparing spectra (a) and (c). Rewarming from (c) to (d) gave no significant new changes.

Figure 7 continues with the heating of the amorphous sample of Figure 7, the changes this time being between 90 and 115 K. In sharp contrast to what is found in Figure 6, this time the changes on warming are both pronounced and irreversible, corresponding to crystallization of the amorphous ice on going from (a) to (b). The differences in peak heights, widths, and shapes on going from 90 to 115 K are obvious. Recooling to 90 K in (c) followed by rewarming to 115 K in (d) gave almost no additional changes, so that spectra (b), (c), and (d) are nearly identical. See Figure 1 of Gálvez et al. (2009) for similar changes, albeit at different temperatures.

Figure 8 further continues the annealing (heating followed by cooling) of the initially amorphous sample of Figure 6, now between 115 and 130 K. No large, significant spectral changes are seen in traces (a) through (d) as the temperature is varied. The lower temperature gives marginally sharper features, but the difference is quite small. In short, once the ice crystallized it did not revert to an amorphous solid on recooling. No such reversal was expected and none was observed.

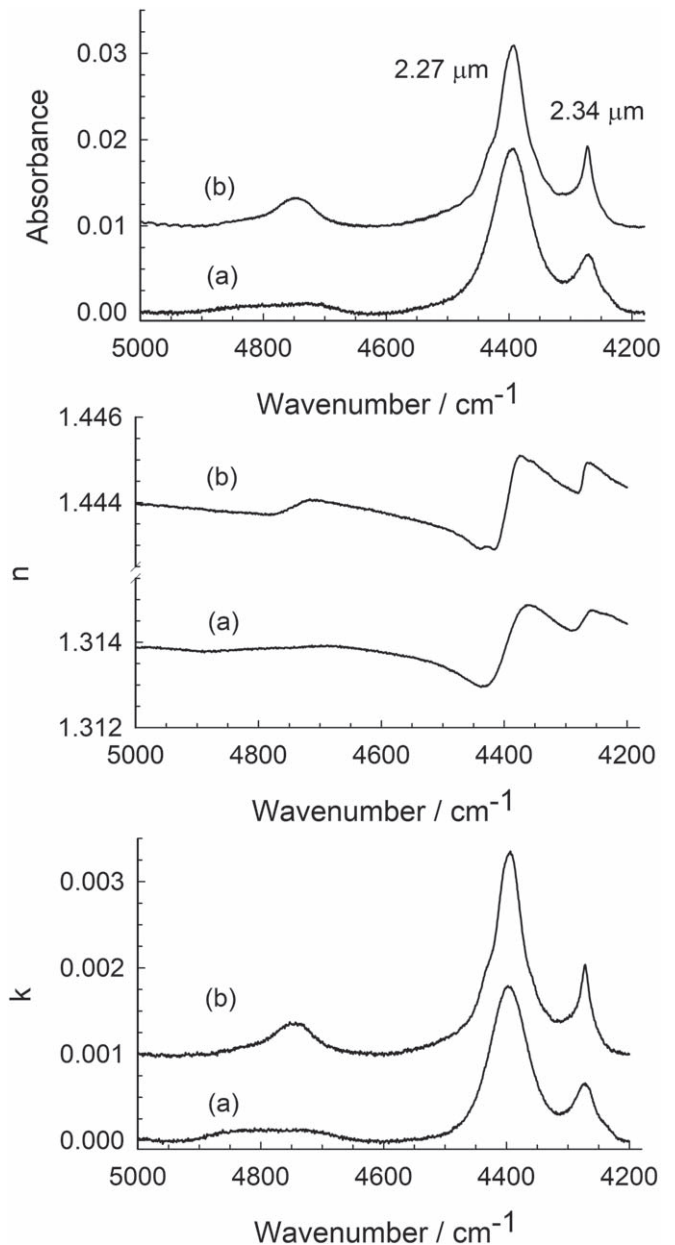


Figure 5. Near-IR spectra and optical constants of two CH_3OH ices, with (a) in each case being for amorphous CH_3OH at 10 K and (b) being for crystalline CH_3OH at 120 K. In the top panel, (b) has been offset by 0.01 on the vertical axis for clarity, with each spectrum being for an ice with a thickness of $3.7\ \mu\text{m}$. In the bottom panel, trace (b) has been offset vertically by 0.001.

5.5. Infrared Spectra of Methanol Solid-phase Transitions

The methanol crystallization of Figure 7 took place in just a few seconds at 120 K, but a few minutes were needed at 115 K. Figure 9 follows the progress of the transition over about 2 hr at 105 K. In the upper panel, an isobestic point at 1140 cm^{-1} suggests, but does not necessarily prove, that the conversion is a straightforward amorphous-to-crystalline change without the intermediacy of any other form of methanol. The lower part of the Figure shows a clear association between the fall of the amorphous ice's IR peak at 1130.7 cm^{-1} and the rise of the crystalline ice's peak at 1143.6 cm^{-1} . More quantitatively, as the fraction of the sample that was amorphous fell to 50%, the fraction of the methanol ice that was crystalline had risen to that same value.

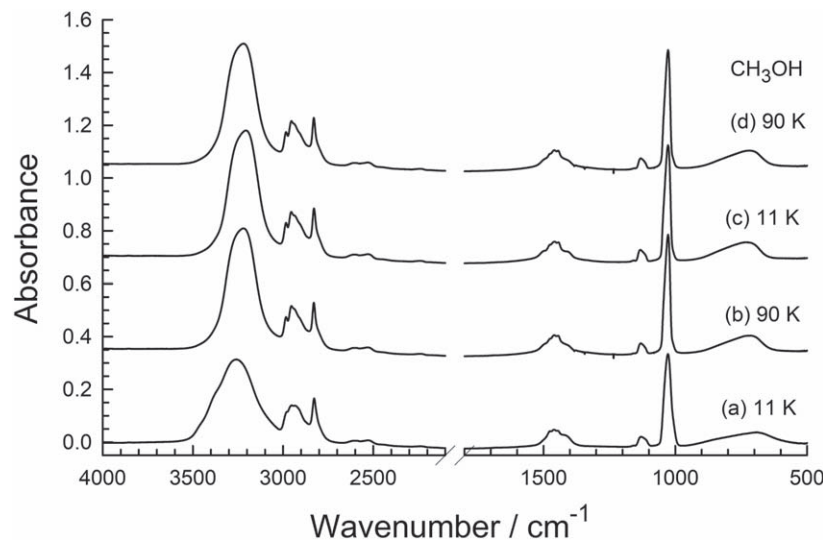


Figure 6. Infrared spectra of methanol (a) condensed at 10 K from CH_3OH vapor, (b) warmed to 90 K, (c) recooled to 10 K, and (d) rewarmed to 90 K. Spectra are offset for clarity. The ice’s initial thickness was about $1 \mu\text{m}$.

Table 8
Intensities of Two Near-IR Absorptions of $\text{CH}_3\text{OH}^{\text{a,b}}$

Peak Position $\bar{\nu}$ / cm^{-1}	Peak Position $\lambda/\mu\text{m}$	$A'/10^{-18} \text{ cm}^{-1}$ molecule $^{-1}$
10 K amorphous CH_3OH		
4398	2.274	0.59
4273	2.340	0.11
120 K crystalline CH_3OH		
4393	2.276	0.50
4272	2.341	0.079

Notes.

^a See Cruikshank et al. (1998) for assignments of the overtones near 4400 cm^{-1} ($2.27 \mu\text{m}$) and 4271 cm^{-1} ($2.34 \mu\text{m}$).

^b Only two significant figures are given for A' due to the relative weakness of each band compared to mid-IR features.

Only a few IR measurements were made with CH_3OH ices above 130 K in part because their astrochemical relevance was unclear, but also because, at those temperatures, the ices underwent sublimation in our vacuum systems. As already mentioned, our crystalline methanol ices were in the lower-temperature (α) form. Some years ago, Falk & Whalley (1961) reported that methanol’s α and β crystalline phases have nearly the same IR spectra. One difference is that the α (lower-temperature) phase has a small, sharp IR peak near 2037.0 cm^{-1} , corresponding to the overtone of the C–O vibration near 1030 cm^{-1} . However, the overtone is near 2043.5 cm^{-1} in the β form of the compound. It was this small, but sharp, feature that we used to investigate the crystalline–crystalline change in methanol.

Our attempts to observe the $\alpha \rightarrow \beta$ change by warming $\alpha\text{-CH}_3\text{OH}$, such as the sample from Figure 8, gave only modest evidence for the conversion. However, success was met when we reversed the process, rapidly condensing CH_3OH at 155 K and then quickly cooling to 140 K to slow the ice’s sublimation. The energy released during the condensation of methanol vapor was sufficient to produce an ice that was largely in the β phase. We then recorded IR spectra of the ice over several hours, clearly observing the $\beta \rightarrow \alpha$ change (i.e., peak at $2043.4 \text{ cm}^{-1} \rightarrow$ peak at 2037.0 cm^{-1}) from the high-

temperature phase to the low-temperature one. See Figure 10. In the upper panel, an isobestic point is obvious at 2040 cm^{-1} suggesting a smooth conversion from one crystalline phase to the other. The lower panel follows the progress of the conversion through the fraction of each form present over time.

5.6. Application #1—Band Strengths in $\text{H}_2\text{O} + \text{CH}_3\text{OH}$ Ices

Interstellar and cometary ices consist of more than one component, and so it is of interest to compare IR band strengths for both neat (i.e., 1 component) ices and ice mixtures dominated by, for example, frozen H_2O . Such measurements are of long-standing interest (e.g., Allamandola et al. 1992), but are difficult due to uncertainties in preparing ice mixtures with accurately known compositions. To address this problem, we recently showed how binary H_2O -rich mixtures of H_2O -ice and H_2S , SO_2 , or OCS can be prepared with compositions that are both accurate and free of assumptions about gas-phase mixtures or spectral intensities (Yarnall & Hudson 2022b). The key to the method was knowing the deposition rate of each component, which required measurements of the density and refractive index of each compound. For the present study, we used this same method to prepare five $\text{H}_2\text{O} + \text{CH}_3\text{OH}$ ices at 10 K each with a molar ratio of 10:1, but with different thicknesses. We recorded the IR spectrum of each sample and measured methanol IR band areas as a function of CH_3OH column density in the sample.

In contrast to our work with H_2O -rich mixtures of sulfur compounds (Yarnall & Hudson 2022b) or HCN (Gerakines et al. 2022), band integrations in $\text{H}_2\text{O} + \text{CH}_3\text{OH}$ ices were severely hindered by the extensive overlap of IR features of the two components of the sample. Figure 11 compares IR spectra of amorphous H_2O -ice and an amorphous $\text{H}_2\text{O} + \text{CH}_3\text{OH}$ (10:1) ice, both ices at 10 K and both having a thickness of about $1 \mu\text{m}$. The IR bands of CH_3OH we selected for measurement in the two-component ice, largely influenced by their use in studying interstellar ices, were near 2830 cm^{-1} ($3.534 \mu\text{m}$), 2580 cm^{-1} ($3.876 \mu\text{m}$), 1128 cm^{-1} ($8.865 \mu\text{m}$), and 1026 cm^{-1} ($9.747 \mu\text{m}$). Baseline issues and uncertainties for integrations have been mentioned by others (Kerkhof et al. 1999). In our study, a quintic polynomial was used to draw a baseline from $\sim 3020\text{--}2750 \text{ cm}^{-1}$, which then allowed us to

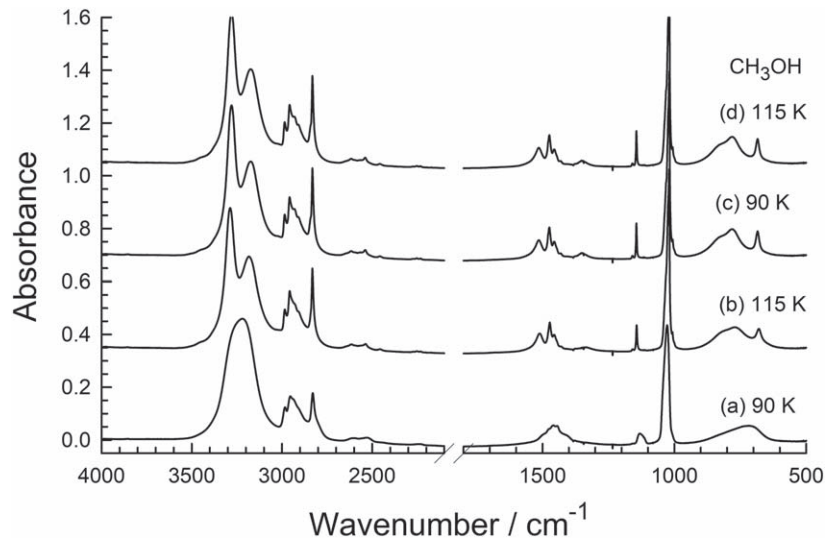


Figure 7. A continuation of the annealing of the methanol ice of Figure 6. The ice was (a) again at 90 K, (b) then warmed to 115 K, (c) then recooled to 90 K, and (d) then rewarmed to 115 K. Spectra are offset for clarity. The ice’s initial thickness was about $1 \mu\text{m}$.

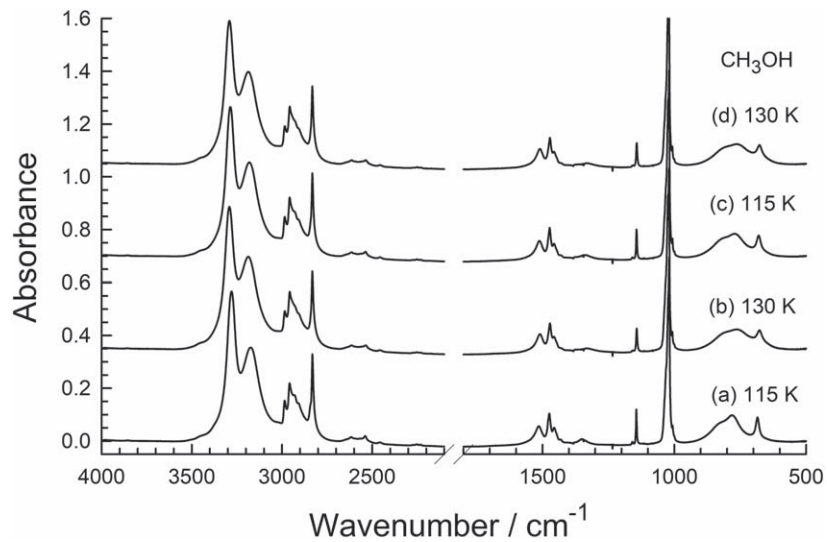


Figure 8. A continuation of the annealing of the methanol ice of Figure 7. The ice was (a) again at 115 K, (b) then warmed to 130 K, (c) then recooled to 115 K, and (d) then rewarmed to 130 K. Spectra are offset for clarity. The ice’s initial thickness was about $1 \mu\text{m}$.

measure (integrate) the IR feature near 2830 cm^{-1} as a function of ice thickness in the usual manner. In the other three IR regions, a simple straight line gave an acceptable baseline ($\sim 2650\text{--}2475 \text{ cm}^{-1}$, $\sim 1180\text{--}1070 \text{ cm}^{-1}$, and $\sim 1070\text{--}980 \text{ cm}^{-1}$). Our ices’ $\text{H}_2\text{O} + \text{CH}_3\text{OH}$ (10:1) composition was a compromise between (a) mixtures with more methanol, making integrations easy but with ices far from interstellar methanol abundances and (b) ice mixtures with such little methanol that accurate integrations of IR bands would have been difficult. See Table 9 for our results, along with a comparison to band strengths of amorphous CH_3OH in those same regions. Correlation coefficients were on the order of 0.998 and above.

5.7. Application #2—Vapor Pressures from IR Measurements

Khanna et al. (1990) described how vapor pressures of ices can be measured with IR spectra, but the method is not widely used. Perhaps the main obstacle is that the density and refractive index of the ice sample must be known, two quantities that were not

specified in the original paper of Khanna et al. (1990). However, since these are the properties we present in Table 3, it seemed reasonable to compare results from the IR method to those from a microbalance method we have used before (Hudson et al. 2022b). For that, we grew four crystalline CH_3OH ices (thickness $\approx 3 \mu\text{m}$) at 120 K and warmed each to initiate sublimation. Infrared spectra were recorded of each ice as it underwent sublimation. To quantify the solid \rightarrow vapor conversion, the CH_3OH overtone band near 2035 cm^{-1} was integrated, this feature being selected as it overlapped less with other IR bands than any other we studied and was relatively sharp. Changes in IR absorbance for ices held at 140, 145, 150, and 155 K are shown in Figure 12, where the increase in sublimation rate with temperature is clear. A Clausius–Clapeyron plot with the unnormalized pressures gave the following equation (correlation coefficient >0.999) with pressure in Torr and temperature in kelvins:

$$\ln(P) = (-5571)\left(\frac{1}{T}\right) + 18.36. \quad (6)$$

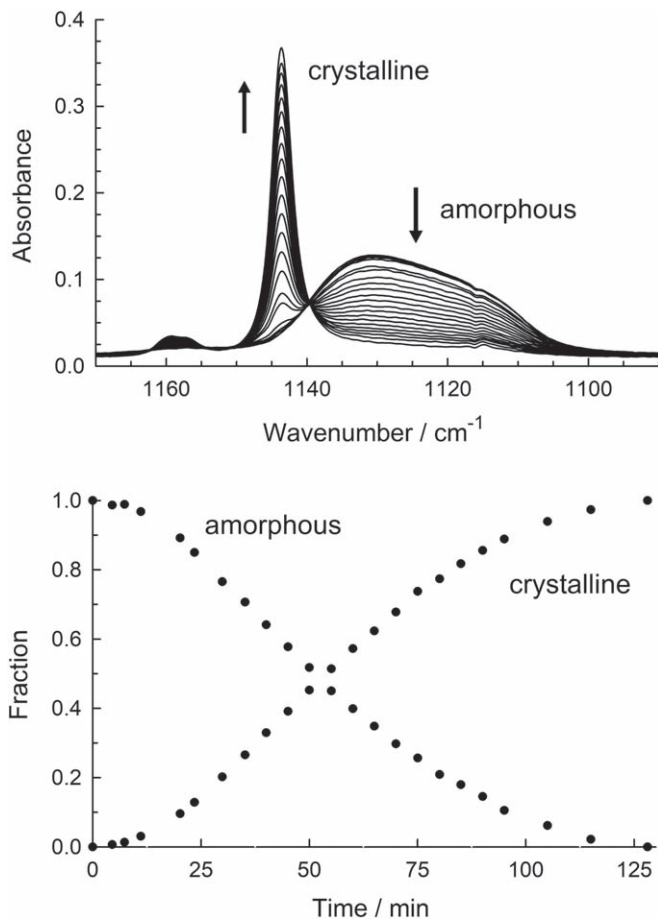


Figure 9. Infrared spectra showing the crystallization of amorphous CH_3OH at 105 K. The ice’s initial thickness was about $3 \mu\text{m}$.

This equation’s slope of $(-\Delta H_{\text{subl}}/R) = -5571 \text{ K}$ gave the enthalpy of sublimation of crystalline methanol as $\Delta H_{\text{subl}} = 46.3 \text{ kJ mol}^{-1}$.

For comparison to these results, we measured vapor pressures in triplicate using our quartz-crystal microbalance. The most accurate values were between about 135 and 155 K, corresponding to a pressure range of about 10^{-7} – 10^{-5} Torr, respectively. Again, a Clausius–Clapeyron plot (correlation coefficient >0.999) prepared from the temperatures and vapor pressures we measured gave the following equation, again with pressure in Torr and temperature in kelvins:

$$\ln(P) = (-5533)\left(\frac{1}{T}\right) + 24.78. \quad (7)$$

The slope of $(-\Delta H_{\text{subl}}/R) = -5533 \text{ K}$ gave the enthalpy of sublimation of crystalline methanol as $\Delta H_{\text{subl}} = 46.0 \text{ kJ mol}^{-1}$. Pressures will be given and compared to a published set in Section 6.

6. Discussion

6.1. Refractive Indices and Ice Densities

Figure 1 shows that a difference exists between the refractive indices and densities we measured for methanol ices and those reported by Luna et al. (2018). Specifically, the refractive indices of Luna et al. (2018) are about 7% lower than ours, while the density differences are closer to 20%. Figure 1 also shows the

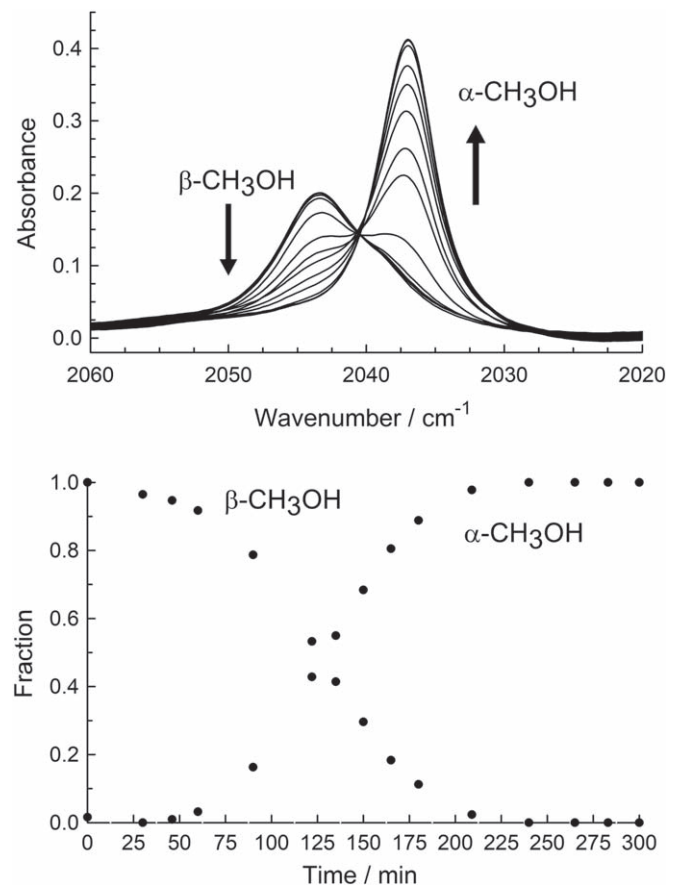


Figure 10. Infrared spectra showing the conversion of the high-temperature (β) phase of crystalline CH_3OH to the lower-phase temperature (α) phase at 140 K.

agreement between our density for crystalline CH_3OH at 120 K and a value based on a diffraction study (Kirchner et al. 2008). Figure 13 compares densities for 13 organic compounds that we measured with a microbalance (Yarnall & Hudson 2022a) with densities reported from diffraction work, the data of which is summarized in Table 10. The disagreement of the Luna et al. (2018) density for methanol with the 120 K literature result and with the overall linear trend in the data is clear, as is the good agreement between those same results and our CH_3OH density.

The low density of Luna et al. (2018) for amorphous CH_3OH was noted earlier by Scirè et al. (2019) in a study of CD_2OH . Those authors applied the Lorentz–Lorenz equation to their own measured refractive index for CH_3OH at 17 K and calculated $\rho = 0.79 \text{ g cm}^{-3}$ compared to the 0.64 g cm^{-3} of Luna et al. (2018). Our value of 0.78 g cm^{-3} agrees with the calculated value of Scirè et al. (2019) for amorphous CH_3OH .

The Lorentz-Lorenz relation can also be applied to crystalline CH_3OH to predict that solid’s refractive index. Combining the room-temperature values of $n = 1.3267$ and $\rho = 0.7864 \text{ g cm}^{-3}$ for methanol (Ortega 1982) with the 122 K density of $\rho = 1.028 \text{ g cm}^{-3}$ for the crystalline solid (Kirchner et al. 2008) gives a predicted refractive index of $n = 1.442$ compared to our $n = 1.444$ at 120 K (Table 3). We conclude that our values of n and ρ for methanol ices agree with expectations for amorphous and crystalline CH_3OH . The reasons for the lower values of Luna et al. (2018) are not known, but we recently have also found a low density for crystalline CO from the same laboratory (Gerakines et al. 2023).

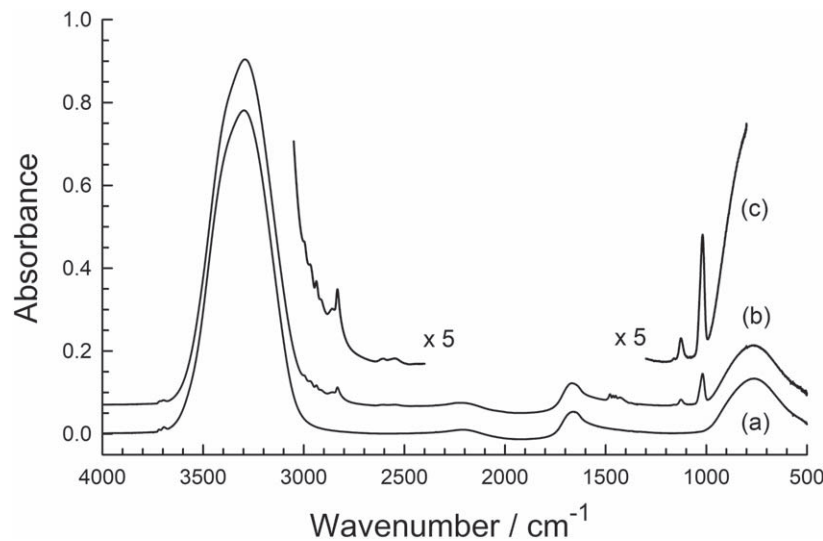


Figure 11. Infrared spectra of amorphous ices at 10 K, each with a thickness of about $1 \mu\text{m}$. (a) H_2O , (b) $\text{H}_2\text{O} + \text{CH}_3\text{OH}$ (10:1), (c) same as (b) but expanded vertically by a factor of 5.

Table 9
Intensities of Three IR Absorptions of CH_3OH -containing Ices at 10 K^a

CH_3OH			$\text{H}_2\text{O} + \text{CH}_3\text{OH}$ (10:1)		
Position(s)/ cm^{-1}	Integration Range/ cm^{-1}	$A'/10^{-18}$ cm molecule $^{-1}$	$A'/10^{-18}$ cm molecule $^{-1}$	Integration Range/ cm^{-1}	Position(s)/ cm^{-1}
2828	2860–2755	5.19	7.01	2890–2770	2833
2592 2526	2685–2338	2.91	1.81	2650–2475	2605 2548
1129	1180–1070	1.90	2.58	1180–1070	1126
1028	1070–970	16.2	14.2	1070–980	1018

Note.

^a A density and refractive index for amorphous H_2O -ice were needed for the accurate preparation of $\text{H}_2\text{O} + \text{CH}_3\text{OH}$ ice mixtures. See Gerakines et al. (2022) for our measurements of $n_{670} = 1.234 \pm 0.008$ and $\rho = 0.719 \pm 0.005$ g cm^{-3} at 19 K.

6.2. Infrared Spectra and Intensities

Our ices' IR spectral positions, band shapes, and relative intensities resemble those of published spectra, such as those in the five works cited in Table 1. A comparison of one of our amorphous CH_3OH spectra to those in the two studies of Table 1 that used a resolution of 1 cm^{-1} is shown in Figure 14, each spectrum being scaled for a thickness of $1 \mu\text{m}$. The upper panel compares our work to the results of Hudgins et al. (1993), and a substantial difference in peak heights is seen. It seems likely that the large peak heights of the Hudgins spectrum arise from a problem with the measurement of ice thickness. Specifically, the red points in Figure 3 correspond to a published thickness of $0.56 \mu\text{m}$, but our Beer's Law line in that same Figure suggests that the measured absorbances of ~ 0.26 correspond to an ice of thickness $\sim 0.80 \mu\text{m}$. The middle panel of Figure 14 shows that a multiplication of absorbance by $0.56/0.80$ brings the two spectra into very close agreement. The bottom panel of Figure 14 adds a spectrum from a figure in Bouilloud et al. (2015) that was sufficiently large for an acceptable digitization and scaling to a thickness of $1 \mu\text{m}$. It agrees with the other spectra shown. Not included is a spectrum from Luna et al. (2018), their spectra being unavailable in digital form and so small in the published figures that digitization is difficult. We simply note that the peak heights in the published spectra of Luna et al. (2018) are slightly

smaller than those in Figure 14, just as expected from the slightly lower resolution used by those authors.

Table 11 compares our band strengths for amorphous CH_3OH to those of Bouilloud et al. (2015) and Luna et al. (2018) after rescaling each with our n - and ρ -values. In four of the five cases shown, the better agreement is with the Bouilloud et al. (2015) results, again as expected. The exception is for a broad band ($\sim 1500 \text{ cm}^{-1}$) for which those authors appear to have used a very large integration range, raising A' . The values of Hudgins now are in much better agreement with the 1 cm^{-1} data of Bouilloud et al. (2015) and the present work, with the lower-resolution (2 cm^{-1}) band strengths of Luna et al. (2018) being somewhat smaller. As already mentioned, the A' -values of Hudgins et al. (1993) were based on spectra of a single amorphous CH_3OH ice of uncertain thickness (see above) and with an unknown integration range.

For crystalline CH_3OH , comparisons were difficult due to the scarcity of data in the literature. The average absolute deviation at 120 K between our band strengths and those of Luna et al. (2018) before and after rescaling with our n - and ρ -values barely changed from 17%. Differences are likely from a combination of ice temperature (10 K versus 20 K), spectral resolution (1 cm^{-1} versus 2 cm^{-1}), and baseline corrections.

In some ways, IR intensities of ices are easier to compare using optical constants than using band strengths because integration ranges and ice densities are not needed. A reference index of

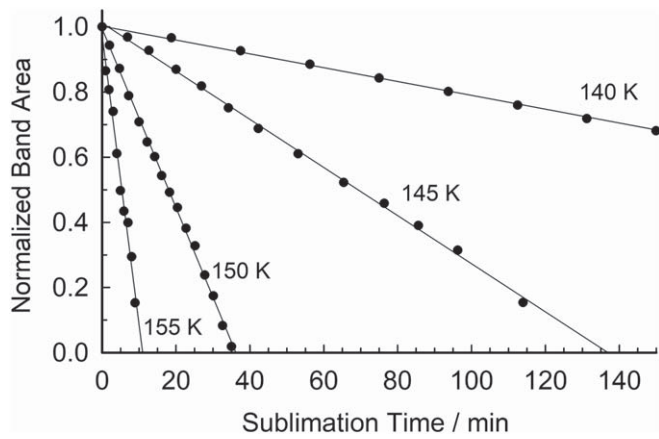


Figure 12. Sublimation of crystalline CH_3OH at four temperatures. The change at 140 K was followed for ~ 230 minutes, but only data for the first 140 minutes are included here to give a slight expansion of the horizontal axis and better show the data points at 150 and 155 K. The IR band integrated was at 2035 cm^{-1} .

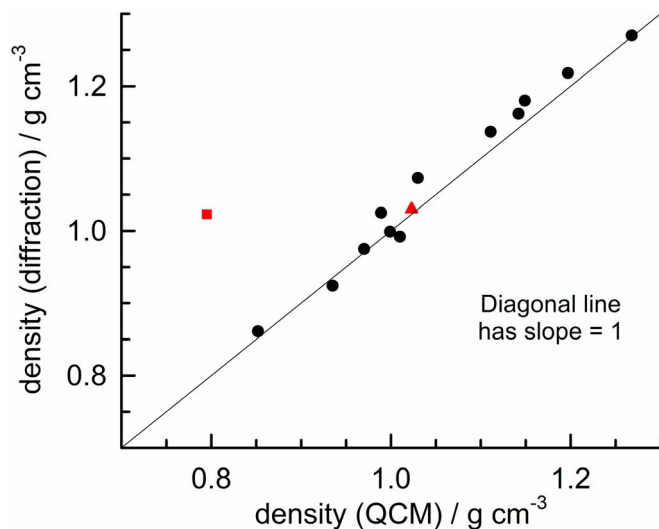


Figure 13. Comparison of crystalline ice densities measured with a quartz-crystal microbalance (QCM) to those in the literature from diffraction studies. Black points: authors' measurements for the compounds in Table 10. Red square: value of Luna et al. (2018) for CH_3OH at 120 K. Red triangle near diagonal line: value of the present authors for CH_3OH at 120 K. See also Yarnall & Hudson (2022a).

refraction is still important for measuring ice thickness and serving as a reference point for Kramers-Kronig calculations, but small changes in the reference n result only in small changes in the final $n(\tilde{\nu})$ - and $k(\tilde{\nu})$ -values across the IR spectrum.

Three refereed papers that reported methanol optical constants are listed in Table 2. For reasons already described, the $n(\tilde{\nu})$ and $k(\tilde{\nu})$ results of Rocha & Pilling (2014) are the least attractive for quantitative comparisons and so are not used for that purpose here, leaving only the constants of Hudgins et al. (1993) and Luna et al. (2018). The upper panel of Figure 15 shows a substantial difference between the $k(\tilde{\nu})$ -values of Hudgins et al. (1993) and our own results. The reasons for these differences are, once more, almost certainly due to the ice thickness of Hudgins et al. (1993) being near $0.80\ \mu\text{m}$ and not the $0.56\ \mu\text{m}$ published. As a correction, we multiplied the absorbance values of Hudgins spectrum by $0.56/0.80 \approx 0.70$ and then recalculated the optical constants with our own

Table 10
Densities and Refractive Indices of Thirteen Crystalline Ices

No.	Formula, Name	This Work ^{a,b}		Literature ^b	
		T	ρ	ρ	T
1	CH_3OH , methanol	120	1.023	1.03 ^c	122
2	$\text{C}_2\text{H}_5\text{OH}$, ethanol	120	0.989	1.025 ^d	87
3	HC(O)CH_3 , acetaldehyde	100	1.111	1.137 ^e	5
4	$(\text{CH}_3)_2\text{CO}$, acetone	125	0.999	0.999 ^f	110
5	CH_3COOH , acetic acid	150	1.268	1.27 ^g	269
6	$\text{CH}_3\text{COOCH}_3$, methyl acetate	115	1.197	1.218 ^h	145
7	$(\text{CH}_3)_2\text{O}$, dimethyl ether	75	0.970	0.975 ⁱ	93
8	$c\text{-OC}_2\text{H}_4$, ethylene oxide	100	1.142	1.162 ^j	100
9	CH_3NH_2 , methylamine	100	0.861	0.852 ^k	123
10	$\text{C}_2\text{H}_5\text{NH}_2$, ethylamine	100	0.924	0.935 ^l	150
11	CH_3CN , acetonitrile	130	1.073	1.030 ^m	201
12	$\text{C}_2\text{H}_5\text{CN}$, propionitrile	110	0.992	1.010 ⁿ	100
13	$\text{C}_5\text{H}_5\text{N}$, pyridine	120	1.149	1.180 ^o	153

Notes.

- ^a See Yarnall & Hudson (2022a) for these values.
^b Temperatures are in kelvins and densities are in g cm^{-3} .
^c Kirchner et al. (2008).
^d Jönsson (1976).
^e Ibberson et al. (2000).
^f Allan et al. (1999).
^g Jones & Templeton (1958).
^h Barrow et al. (1981).
ⁱ Vojinovic et al. (2004).
^j Grabowsky et al. (2008).
^k Atoji & Lipscomb (1953).
^l Maloney et al. (2014).
^m Enjalbert & Galy (2002).
ⁿ Brand et al. (2020).
^o Mootz & Wussow (1981).

computer code (Gerakines & Hudson 2020). The results, seen in the lower panel of Figure 15, are in close agreement with our own. Luna et al. (2018) noted a similar discrepancy, but no explanation was offered. As for their own $k(\tilde{\nu})$ -values for amorphous CH_3OH , they are slightly lower than ours near 10 K, but such a difference is again expected from the lower resolution those authors used.

None of the papers cited in Tables 1 and 2 reported optical constants at 1 cm^{-1} resolution for crystalline methanol ice made by condensation at 120 K, such as in Figure 2. The closest is, again, the work of Luna et al. (2018) who condensed methanol at 120 K, but with spectra recorded at 2 cm^{-1} resolution. Their k -values for the intense IR peaks near 3300 and 1020 cm^{-1} are about 10% less than ours. As already mentioned, comparisons are difficult due to a lack of spectra and optical constants in digital form, in addition to the lack of the computer routine used by those authors and the small scale of their figure with eight overlapping spectral traces. The $k(\tilde{\nu})$ -values for those same two peaks, near 3300 and 1020 cm^{-1} , are about 30% smaller than those given by Hudgins et al. (1993) for an ice grown at 10 K and warmed to 120 K.

6.3. Near-IR Spectra and Band Strengths

The only direct measurements we have found of solid-methanol's near-IR band strengths are those of Luna et al. (2018), who recorded spectra of ices formed at eight temperatures, but with only one spectrum at each temperature and with an ice thickness of $\sim 3.4\ \mu\text{m}$. In contrast, we measured

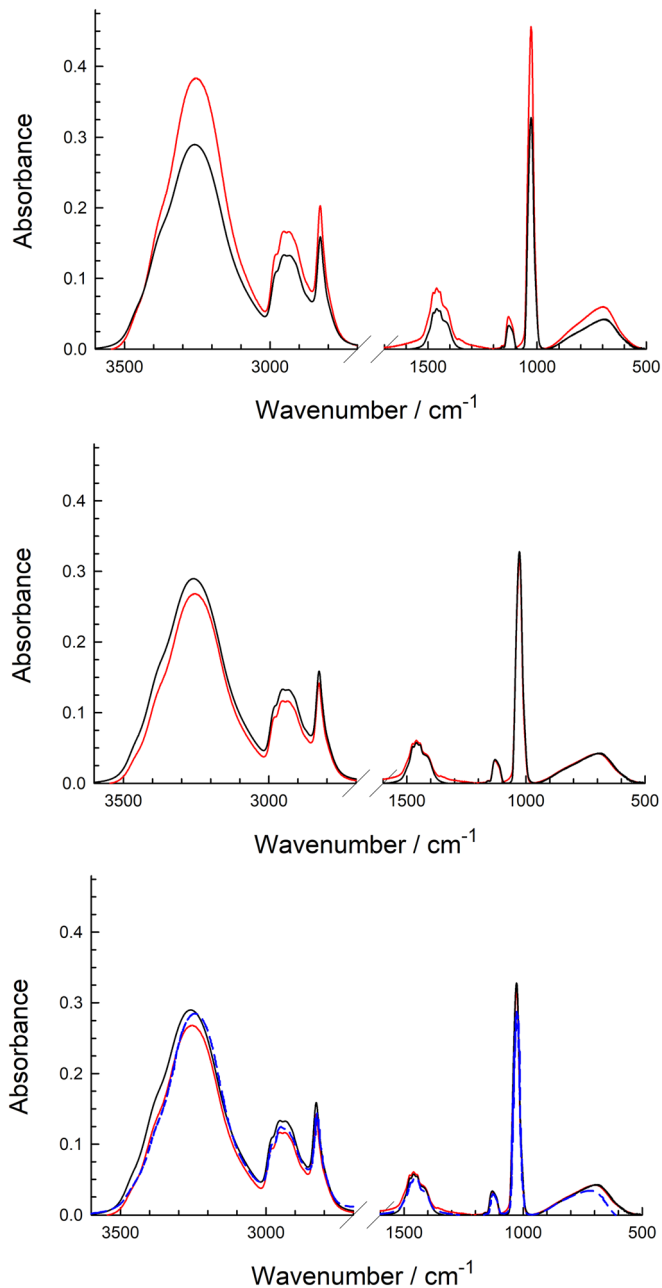


Figure 14. Infrared spectra of amorphous CH_3OH ices at 1 cm^{-1} resolution and a thickness of $1\ \mu\text{m}$. Black lines: 10 K spectrum from this work. Red lines: 10 K spectrum of Hudgins et al. (1993) before (upper) and after (middle and lower) scaling the thickness as described in the text. Dashed blue line (bottom): spectrum of an ice at 25 K from Bouilloud et al. (2015), digitized and scaled to a thickness of $1\ \mu\text{m}$.

near-IR band strengths at just 10 and 120 K, but with ices having thicknesses from about $1\text{--}8\ \mu\text{m}$ so as to construct Beer’s Law plots and extract band strengths. Our results are in Table 8 for the two IR bands of interest. Our A' -values are higher than those of Luna et al. (2018), such as $\sim 8\%$ larger than for the band near 4398 cm^{-1} in amorphous CH_3OH , but differences can again be expected, as those authors’ results were based on just one ice and at a lower resolution, and with no details about curve fitting or a choice of baseline.

Our near-IR results for CH_3OH ices appear to be the first of their kind. Indirect measurements made by ratioing intensities of near-IR features to a mid-IR band have been reported by

Table 11
IR Band Strengths of Amorphous Methanol Ices^a

Region/ cm^{-1}	This Work (2023) ^b	Hudgins et al. (1993) Recalculated ^c	Bouilloud et al. (2015) Recalculated ^d	Luna et al. (2018) Recalculated ^e
3650–2685	152	146	151	120
2685–2338	2.91	2.55	2.66	2.31
1656–1310	7.69	10.6	9.77	6.79
1180–1070	1.91	1.64	2.09	1.14
1070–967	16.2	16.4	16.0	13.2

Notes.

^a Band strengths given as $A'/10^{-18}\text{ cm molecule}^{-1}$.

^b Ices made and spectra recorded at 10 K at a resolution of 1 cm^{-1} .

^c Authors’ spectrum at 1 cm^{-1} resolution for 10 K ice. The authors’ results have been reanalyzed with a density of $\rho = 0.779\text{ g cm}^{-3}$ and a correction has been made to the ice’s thickness as described in the text. No integration limits were provided by the authors. Original values were published with two significant figures.

^d Ices made and spectra recorded at 25 K at a resolution of 1 cm^{-1} . The authors’ published A' -values have been rescaled using the n - and ρ -values at 15 K in this work. No integration limits were provided by the authors.

^e Ices made and spectra recorded at 20 K at a resolution of 2 cm^{-1} . The authors’ published A' -values have been rescaled using the n - and ρ -values at 15 K in this work. The integration limits used by the authors were similar to those in the first column.

Sandford & Allamandola (1993) and by Gerakines et al. (2005), but the reference band strength used in each paper was taken from the early work of d’Hendecourt & Allamandola (1986), about which we already have described problems and concerns. Each of the two newer studies involved measuring IR spectra of multiple ices, but no integration limits, no details about a baseline for integrations, and no details about curve fitting were provided, hindering meaningful quantitative comparisons.

6.4. Changes with Temperature and Time in CH_3OH Ices

The trends in Figures 6–8 from annealing cycles resemble those described, but not illustrated with spectra, by Hagen et al. (1981) on H_2O -ice. Our warming of amorphous CH_3OH from 10 K produced irreversible changes in the ice’s IR spectrum, a situation that did not change until the ice crystallized. We note that the IR spectrum of crystalline CH_3OH has a slight dependence on the way the solid is made, such as by warming from $10\text{--}120\text{ K}$ compared to vapor-phase deposition at 120 K. The differences can be attributed to variations in the size and shape of the crystals grown by the two methods.

Figures 9 and 10 show spectral changes observed when a CH_3OH ice was held at 105 and 140 K, respectively, the first change being for crystallization of amorphous methanol and the second being for the $\beta \rightarrow \alpha$ phase change. No evidence for intermediate forms or phases of methanol was found in either case. Similarly, the sublimation of α - CH_3OH ices held at $140\text{--}155\text{ K}$ proceeded smoothly, with no evidence of the liquefaction seen with ethanol, $\text{CH}_3\text{CH}_2\text{OH}$ (Hudson 2017).

6.5. $\text{H}_2\text{O} + \text{CH}_3\text{OH}$ Ices

Given the importance and prevalence of amorphous $\text{H}_2\text{O} + \text{CH}_3\text{OH}$ ices, it is surprising that so few methanol band strengths exist for such mixtures. In fact, the only measurement of IR band strengths of $\text{H}_2\text{O} + \text{CH}_3\text{OH}$ ices we have found is that of Kerkhof et al. (1999). Their method, like ours, involved

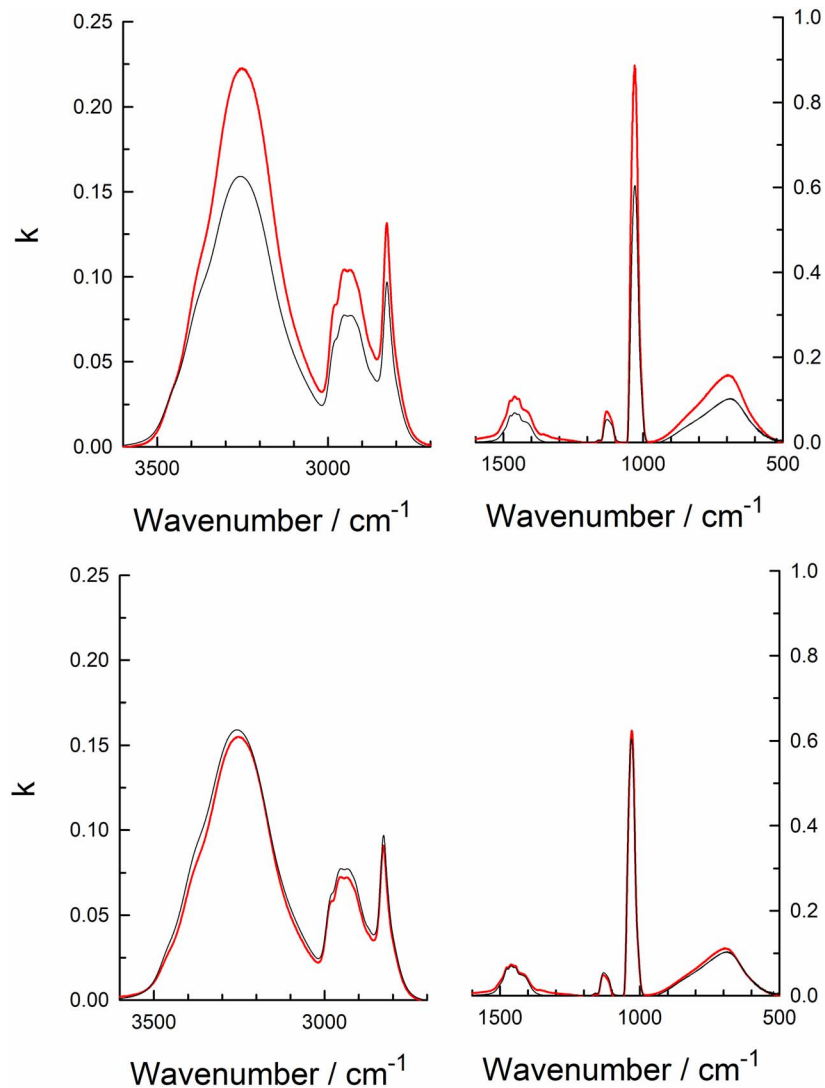


Figure 15. Comparisons of the IR optical constants $k(\tilde{\nu})$ for amorphous CH_3OH ice near 10 K from this work (black lines) and from Hudgins et al. (1993; red lines). The upper panel shows the results of Hudgins et al. (1993) as published. The lower panel has the Hudgins et al. (1993) result after the thickness correction described in the text was applied and the optical constants recalculated.

vapor-phase condensation of the two compounds through separate transfer tubes onto a pre-cooled substrate. However, while we used interference fringes and measured n - and ρ -values for each component to determine that compound's abundance in the resulting ice, Kerkhof et al. (1999) were forced to rely on the solid-phase band strengths available at the time (Hudgins et al. 1993). The disadvantage of that approach is that those same band strengths suffered from the problems already described, such as an unknown density of amorphous methanol. Moreover, no integration limits were reported by Kerkhof et al. (1999), so that it is not certain that the same IR regions were integrated as in the Hudgins et al. (1993) reference spectra (work that also did not give integration limits). These difficulties are readily seen with the benefit of hindsight, so we emphasize that the method of Kerkhof et al. (1999) should give good results if better band strengths are used, such as in Table 4, and if ices with multiple thicknesses are examined. For the present, however, the results of Table 9 are the first and only data of their type.

6.6. Observations and Applications with JWST and Other Facilities

The conditions we have selected for our measurements were made specifically with an eye on JWST's capabilities and what is known of interstellar ices. Our 1 cm^{-1} resolution resembles that of JWST's NIRSpec instrument near 3200 cm^{-1} , the four IR regions of Table 9 are those often used to extract methanol-ice abundances (Boogert et al. 2015), and the 10:1 $\text{H}_2\text{O}:\text{CH}_3\text{OH}$ is a reasonable value for interstellar ices.

Table 9 shows that there is a difference between the IR band strengths of amorphous CH_3OH in the presence and absence of H_2O -ice, a difference that is beyond the 5% uncertainty that we claim for band strengths. A legitimate, robust comparison of our A' -values for ice mixtures to those from previous publications cannot be made, as all earlier results had to contend with the uncertainties already mentioned, as well as some procedural choices that we do not recommend. For now, we can say that the band strengths of $\text{H}_2\text{O} + \text{CH}_3\text{OH}$ ices in Table 9 are the most accurate available and the only ones of their kind. We can

Table 12
Vapor Pressures of Crystalline Methanol^a

T/K	$P/10^{-8}$ Torr This Work, IR	$P/10^{-8}$ Torr This Work, UHV	$P/10^{-8}$ Torr Literature ^b
155	1710	1810	2400
150	514	550	711
145	146	154	194
140	36.1	39.5	53.8
135	... ^c	9.13	13.7

Notes.

^a Vapor pressures rounded to three significant figures. Values at other temperatures can be found by using Equations (6) and (7). Vapor pressure uncertainties are about 1%. See the text.

^b Lucas et al. (2005).

^c Not measured at 135 K.

confidently recommend them for analyzing spectra from JWST and other IR-capable facilities.

As an example of an application, we again consider the recent JWST observations of McClure et al. (2023). The methanol band observed near 1025 cm^{-1} ($9.76\text{ }\mu\text{m}$) was used to calculate a CH_3OH column density by adopting a band strength of $A'(1025\text{ cm}^{-1}, 9.76\text{ }\mu\text{m}) = 1.8 \times 10^{-17}\text{ cm molecule}^{-1}$ for anhydrous methanol. Although Bouilloud et al. (2015) was cited, that A' actually is from Hudgins et al. (1993). The band strength adopted was for “dry” methanol and is about 26% larger than what we have measured, $A' = 1.42 \times 10^{-17}\text{ cm molecule}^{-1}$ for CH_3OH in the presence of H_2O -ice. Adopting our smaller band strength will result in a larger methanol column density.

6.7. Vapor Pressures

Table 12 lists vapor pressures for crystalline CH_3OH obtained by our IR and UHV measurements and by a mass spectrometric technique of Lucas et al. (2005). Our two sets of values are in reasonable agreement, with the UHV vapor pressures being on average $\sim 7\%$ higher than those from the IR-based measurements, a difference that could arise from a 120 K band strength for methanol being used for work at 140, 145, 150, and 155 K. We also found agreement between the sublimation enthalpies for the two experiments, each being about 46 kJ mol^{-1} . Additional IR measurements would be useful in reducing uncertainties and extending the temperature range of the vapor pressures, but we can already conclude that the vapor-pressure method proposed by Khanna et al. (1990) works well for methanol.

The best literature comparison to our methanol vapor pressures in Table 10 is from Lucas et al. (2005), who measured vapor pressures with a mass spectrometer. Their pressures are about 1.35 times larger than ours in the 135–155 K region. Those same authors reported a sublimation enthalpy of 42.9 kJ mol^{-1} for 130–145 K and 46.9 kJ mol^{-1} for 145–157 K, for an average of 44.9 kJ mol^{-1} , in reasonable agreement with our $\Delta H_{\text{subl}} = 46.0\text{ kJ mol}^{-1}$.

For the present, we recommend Equation (7), based on our QCM data, for vapor pressures in the 135–155 K region. The microbalance method we used is relatively fast and productive, giving a set of temperature/pressure data points for a single ice, in contrast to the IR method, which gives only one vapor pressure for each ice.

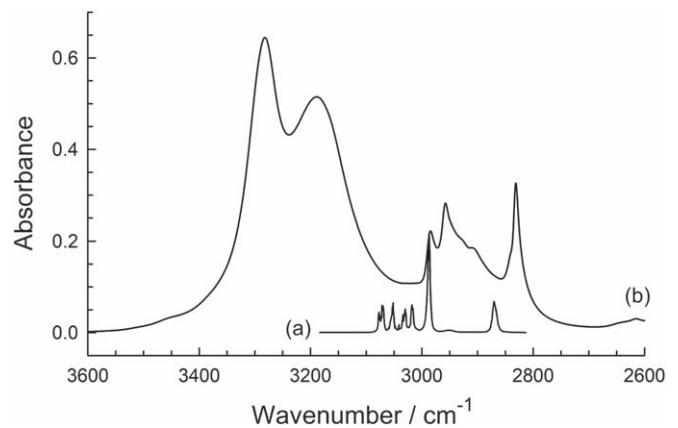


Figure 16. Comparison of (a) simulated and (b) laboratory spectra of crystalline CH_3OH near 130 K. Spectrum (a) is from Nag et al. (2023) and spectrum (b) is from this work. The peaks near 3000 cm^{-1} have been scaled to the same height.

6.8. Comments on Two Recent Publications

The literature on CH_3OH ices continues to grow, as shown by the fact that two relevant papers were published as the present work was being completed. One paper (Nag et al. 2023) included the calculation of IR spectra of crystalline methanol, while the other examined, among other things, spectral changes with temperature (Carrascosa et al. 2023).

The paper of Nag et al. (2023) included simulations of crystalline CH_3OH infrared spectra, but only one figure, Figure 1(c), overlaid simulated and laboratory spectra. The provenance of the chosen laboratory sample and spectrum (i.e., resolution, sample temperature, condensation rate, ice thickness) was not stated, but the spectrum is clearly from amorphous CH_3OH , as it lacks crystalline methanol’s splitting at $3300\text{--}3200\text{ cm}^{-1}$ (see Figure 2(d)). As a comparison of simulated and observed spectra of crystalline methanol was not shown, in Figure 16 we present one, the simulated spectrum being digitized from the supplementary material of Nag et al. (2023). Those same authors spoke of “excellent agreement” between the simulated and the observed spectra. We leave it to readers to decide.

The recent paper of Carrascosa et al. (2023) presented IR spectra of CH_3OH made at different temperatures and of an ice that was warmed from 30–125 K. The results resemble those in Figures 2 and 6–8, but without our annealing cycles. Carrascosa et al. (2023) also showed changes in relative IR intensities of crystalline CH_3OH with ice thickness. The results of that paper are in good qualitative agreement with those presented here. The points of disagreement are quantitative ones, partly from the lower spectral resolution (2 cm^{-1}) of those authors and the assumed values of n and ρ that were interpolated from earlier measurements, about which we already have raised questions (Figure 1). As an example of a quantitative difference, Table 6 has $A'(\sim 3600\text{--}2700\text{ cm}^{-1}) \approx 1.8 \times 10^{-16}\text{ cm molecule}^{-1}$ at 80 K, but Figure 6 of Carrascosa et al. (2023) shows $A'(\sim 3600\text{--}2700\text{ cm}^{-1}) \approx 2.3 \times 10^{-16}\text{ cm molecule}^{-1}$, a difference at least partially due to the smaller density assumed by those authors.

We also note an ambiguity in that same paper concerning agreement with earlier work. The amorphous-methanol band strength reported for 30 K, $A'(\sim 3600\text{--}2700\text{ cm}^{-1}) = 2.3 \times 10^{-16}\text{ cm molecule}^{-1}$, is said to, “not differ from the one at 10 K.” We have not found the study to which that phrase

refers. It also is not clear that a Beer's Law plot was used to determine the authors' reference band strength at 30 K for methanol or if only a single ice was used. Finally, the authors report that for methanol, "the appearance of an intense IR peak at 1299 cm^{-1} is remarkable," but we have not encountered any such peak for methanol either in our laboratory or in the literature, including the present manuscript.

7. Summary and Conclusions

Our investigation of solid CH_3OH has produced some results that are at odds with earlier studies, some results that agree with previous work, and some results that are the first of their type. Our most important new result is that we have examined the sources of long-standing disagreements among different laboratories over IR band strengths of methanol ices and have presented an analysis and corrections that reconcile those differences. Good agreement now exists among the various sets of IR band strengths (A'), especially between ours and the older work at the same IR resolution. The serendipitous result is that although the referred literature contains significant disagreements in the IR intensities of methanol, our corrections, calculations, and measurements with new n - and ρ -values, a Beer's Law calibration curve, and a rescaling of older work yield lab-to-lab differences in A' on the order of only about 10%. Reducing this value will be difficult due to the lack of relevant details in some of the earlier work.

Our reconciliation of new and published results was considerably aided by new measurements of n and ρ that agree with the trend shown by others, but those for crystalline methanol are better aligned with expectations from diffraction studies.

Reversible and irreversible changes in the IR spectra of methanol ices with temperature have been demonstrated with annealing experiments, as opposed to only spectra of ices being warmed or cooled. Our qualitative results include the demonstration that annealing amorphous CH_3OH gives only slight, but definite, irreversible spectral changes until crystallization is achieved. Warming of a crystalline sample under vacuum gave sublimation with no indication of liquefaction from IR spectra.

In the near-IR region, we carried out the first determinations of band strengths of methanol ices using multiple ice samples and a Beer's Law treatment. Our results should be useful to observational astronomers seeking evidence of solid CH_3OH on TNOs and perhaps other objects.

We have prepared both the α and β forms of crystalline CH_3OH and examined the β -to- α conversion at 140 K. The formation of α - CH_3OH is sufficiently rapid, and the temperature high enough for sublimation, that we do not expect β - CH_3OH to have any significant astrochemical importance.

We also are reporting the first IR band strengths for an $\text{H}_2\text{O} + \text{CH}_3\text{OH}$ mixture in which the ice's composition is determined accurately by a method involving independent deposition lines and the underlying properties of each component. The difficulty of making $\text{H}_2\text{O} + \text{CH}_3\text{OH}$ ices of known composition has been considerably reduced so that we can report, for the first time, accurate band strengths of $\text{H}_2\text{O} + \text{CH}_3\text{OH}$ ices at 10 K in the IR regions accessible to JWST.

The literature on IR optical constants and band strengths of CH_3OH ices has long been dominated by the early study of Hudgins et al. (1993), but with which subsequent work disagreed (Luna et al. 2018). By using a calibration curve

(i.e., Beer's Law plot), we have determined that the Hudgins et al. (1993) results, being based on just one ice, need a slight correction for thickness, after which there is good agreement among laboratory results from various researchers.




As an application of our new methanol data, we have measured vapor pressures and a sublimation enthalpy of crystalline CH_3OH using IR spectra. The results were within $\sim 7\%$ of those from independent determinations with a quartz-crystal microbalance, boosting confidence in the IR method for vapor-pressure measurements.

Tables 1 and 2 illustrate an important point on which we end. Accurate, quantitative measurements of IR spectra are challenging, and their application to problems of extraterrestrial chemistry can be even more so. However, omission of underlying data (e.g., n , ρ) and the lack of electronic sharing of data and computer codes unnecessarily complicate inter-laboratory comparisons, hindering their application to astronomical problems. Scirè et al. (2019) pointed out that inter-laboratory comparisons can be difficult, but we do not believe that they should be.

Acknowledgments

We acknowledge the support of NASA's Planetary Science Division Internal Scientist Funding Program through the Fundamental Laboratory Research (FLaRe) work package at the NASA Goddard Space Flight Center with additional funding from the NASA Astrobiology Institute's Goddard Center for Astrobiology. We were assisted in some early methanol measurements by a summer intern, Tatiana Tway (Delaware Valley University), who was supported by the DREAM program at the NASA Goddard Space Flight Center and NASA's SSERVI program. A second summer student, Ella Mullikin (Wellesley College), assisted with some exploratory work with $\text{H}_2\text{O} + \text{CH}_3\text{OH}$ ices. She was supported by the Goddard Center for Astrobiology.

ORCID iDs

Reggie L. Hudson  <https://orcid.org/0000-0003-0519-9429>
 Perry A. Gerakines  <https://orcid.org/0000-0002-9667-5904>
 Yukiko Y. Yarnall  <https://orcid.org/0000-0003-0277-9137>

References

- Allamandola, L. J., Sandford, S. A., & Valero, G. J. 1988, *Icar*, **76**, 225
 Allamandola, L. J., Sandford, S. A., Tielens, A. G. G. M., & Herbst, T. M. 1992, *ApJ*, **399**, 134
 Allan, D. R., Clark, S. J., Ibberson, R. M., et al. 1999, *ChCom*, 1999, 751
 Atoji, M., & Lipscomb, W. N. 1953, *AcCry.*, **6**, 770
 Ball, J. A., Gottlieb, C. A., Lilley, A. E., & Radford, H. E. 1970, *ApJ*, **162**, L203
 Barrow, M. J., Craddock, S., Ebsworth, E. A. V., & Rankin, D. W. H. 1981, *J. Chem. Soc., Dalton Trans.*, 1981, 1988
 Bennett, C. J., Chen, S.-H., Sun, B.-J., Chang, A. H. H., & Kaiser, R. I. 2007, *ApJ*, **660**, 1588
 Bockelée-Morvan, D., Colom, P., Crovisier, J., Despois, D., & Pabert, G. 1991, *Natur*, **350**, 318
 Boogert, A. C. A., Gerakines, P. A., & Whittet, D. C. B. 2015, *ARA&A*, **53**, 541
 Bouilloud, M., Fray, N., Bénilan, Y., et al. 2015, *MNRAS*, **451**, 2145
 Brand, H. E. A., Gu, Q., Kimpton, J. A., Auchettl, & Ennis, C. 2020, *JSynR*, **27**, 212
 Brunetto, R., Baratta, G. A., Domingo, M., & Strazzula, G. 2005, *Icar*, **175**, 226
 Carlson, H. G., & Westrum, E. F. 1971, *JChPh*, **54**, 1464
 Carrascosa, H., Satorre, M. Á., Escibano, B., Martín-Doménech, R., & Muñoz Caro, G. M. 2023, *MNRAS*, **525**, 2690
 Cruikshank, D. P., Roush, T. L., Bartholemew, M. J., et al. 1998, *Icar*, **135**, 389
 d'Hendecourt, L. B., & Allamandola, L. J. 1986, *A&ASS*, **64**, 453

- Dempster, A. B., & Zerbi, G. 1971, *JChPh*, **54**, 3600
- Drobyshev, A., Aldiyarov, A., & Sokolov, D. 2019, *LTP*, **45**, 441
- Enjalbert, R., & Galy, J. 2002, *AcCrB*, **B58**, 1005
- Falk, M., & Whalley, E. 1961, *JPhCh*, **34**, 1554
- Fischer, F., & Fuhrich, R. 1983, *ZNatA*, **38**, 31
- Gálvez, Ó., Maté, B., Martín-Llorente, B., Herrero, V., & Escribano, R. 2009, *JPCA*, **113**, 3321
- Gerakines, P. A., & Hudson, R. L. 2015a, *ApJL*, **805**, L20
- Gerakines, P. A., & Hudson, R. L. 2015b, *ApJL*, **808**, L40
- Gerakines, P. A., & Hudson, R. L. 2020, *ApJ*, **901**, 52
- Gerakines, P. A., Bray, J. J., Davis, A., & Richey, C. R. 2005, *ApJ*, **620**, 1140
- Gerakines, P. A., Materese, C. K., & Hudson, R. L. 2023, *MNRAS*, **522**, 3145
- Gerakines, P. A., Yarnall, Y. Y., & Hudson, R. L. 2022, *MNRAS*, **509**, 3515
- Giuliano, B. M., Escribano, R. M., Martín-Doménech, R., Dartois, E., & Muñoz Caro, G. M. 2014, *A&A*, **565**, A108
- Grabowsky, S., Weber, M., Buschmann, J., & Luger, P. 2008, *AcCry*, **B64**, 397
- Groner, P., Stolkin, I., & Günthard, H. H. 1973, *JPhE*, **6**, 122
- Günzler, H., & Gremlich, H.-U. 2002, *IR Spectroscopy: An Introduction* (Weinheim: Wiley-VCH), 83
- Hagen, W., Tielens, A. G. G. M., & Greenberg, J. M. 1981, *CP*, **56**, 367
- Heavens, O. S. 2011, *Optical Properties of Thin Solid Films* (2nd ed.; New York: Dover), 114
- Hidaka, H., Watanabe, N., Shiraki, T., Nagaoka, A., & Kouchi, A. 2004, *ApJ*, **614**, 1124
- Hollenberg, J. L., & Dows, D. A. 1961, *JChPh*, **34**, 1061
- Hudgins, D. M., Sandford, S. A., Allamandola, L. J., & Tielens, A. G. G. M. 1993, *ApJS*, **86**, 713
- Hudson, R. L. 2017, *AcSpA*, **187**, 82
- Hudson, R. L., & Moore, M. H. 1999, *Icar*, **140**, 451
- Hudson, R. L., & Moore, M. H. 2000, *Icar*, **145**, 661
- Hudson, R. L., & Yarnall, Y. Y. 2022, *ESC*, **6**, 1163
- Hudson, R. L., Ferrante, R. F., & Moore, M. H. 2014a, *Icar*, **228**, 276
- Hudson, R. L., Gerakines, P. A., & Moore, M. H. 2014b, *Icar*, **243**, 148
- Hudson, R. L., Gerakines, P. A., & Yarnall, Y. Y. 2022a, *ApJ*, **925**, 156
- Hudson, R. L., Loeffler, M. J., Ferrante, R. F., Gerakines, P. A., & Coleman, F. M. 2020, *ApJ*, **891**, 22
- Hudson, R. L., Loeffler, M. J., & Gerakines, P. A. 2017, *JChPh*, **146**, 024304
- Hudson, R. L., Yarnall, Y. Y., & Gerakines, P. A. 2022b, *PSJ*, **3**, 120
- Ibberson, R. M., Yamamuro, O., & Matsuo, T. 2000, *JMoSt*, **520**, 265
- Jones, E. E., & Templeton, D. H. 1958, *AcCry*, **11**, 484
- Jönsson, P. 1976, *AcCrB*, **B32**, 232
- Kerkhof, O., Schutte, W. A., & Ehrenfreund, P. 1999, *A&A*, **346**, 990
- Khanna, R. K., Allen, J. E., Masterson, C. M., & Zhao, G. 1990, *JPhCh*, **94**, 440
- Kirchner, M. T., Das, D., & Boese, R. 2008, *Cryst. Growth Des.*, **8**, 763
- Lin, T., Hsing, C., Wei, C., & Kuo, J. 2016, *PCCP*, **18**, 2736
- Lu, C. S., & Lewis, O. 1972, *JAP*, **43**, 4385
- Lucas, S., Ferry, D., Demirdjijan, B., & Suzanne, J. 2005, *JPCB*, **109**, 18103
- Luna, R., Molpeceres, G., Ortigoso, J., et al. 2018, *A&A*, **617**, A116
- Maloney, A. G. P., Wood, P. A., & Parsons, S. 2014, *CrystEngComm*, **16**, 3867
- Materese, C. K., Gerakines, P. A., & Hudson, R. L. 2021, *Acc. Chem. Res.*, **54**, 280
- McClure, M. K., Rocha, W. R. M., Pontopiddan, K. M., et al. 2023, *NatAs*, **7**, 431
- Moore, M. H., Ferrante, R. F., Moore, W. J., & Hudson, R. 2010, *ApJS*, **191**, 96
- Moore, M. H., & Hudson, R. L. 1998, *Icar*, **135**, 518
- Mootz, D., & Wussow, H. G. 1981, *JChPh*, **75**, 1517
- Nag, S., Majumdar, J., Sivaraman, B., Yashonath, S., & Maiti, P. K. 2023, *MNRAS*, **522**, 3656
- Ortega, J. 1982, *J. Chem. Eng. Ref. Data*, **27**, 312
- Palumbo, M. E., Castorina, A. C., & Strazzulla, G. 1999, *A&A*, **342**, 551
- Parks, G. S. 1925, *JACS*, **47**, 338
- Quirico, E., & Schmitt, B. 1997, *Icar*, **127**, 354
- Rocha, W. R. M., & Pilling, S. 2014, *SpeAc*, **123**, 436
- Sandford, S. A., & Allamandola, L. J. 1993, *ApJ*, **417**, 815
- Scirè, C., Urso, R. G., Fulvio, D., Baratta, G., & Palumbo, M. E. 2019, *SpeAc*, **219**, 288
- Snyder, L. E., Buhl, D., Zuckerman, B., & Palmer, P. 1969, *PhRvL*, **22**, 679
- Tauer, K. J., & Lipscomb, W. N. 1952, *AcCry*, **5**, 606
- Tempelmeyer, K. E., & Mills, D. W. 1968, *JAP*, **39**, 2968
- Torrie, B. H., Binbrek, O. S., Strauss, M., & Swainson, I. P. 2002, *JSSCh*, **166**, 415
- Torrie, B. H., Weng, S., & Powell, B. M. 1988, *MolPh*, **67**, 575
- Vojinovic, K., Losehand, U., & Mitzel, N. W. 2004, *J. Chem. Soc. Dalton Trans.*, **16**, 2578
- Yarnall, Y. Y., & Hudson, R. L. 2022a, *Icar*, **373**, 114799
- Yarnall, Y. Y., & Hudson, R. L. 2022b, *ApJL*, **91**, L4